JGR Atmospheres

RESEARCH ARTICLE
10.1029/2022JD036974

Long-Range Transport and Evolution of Saharan Dust Over East Asia From 2007 to 2020

Qiantao Liu[1], Zhongwei Huang[1,2], Zhiyuan Hu[3,4], Qingqing Dong[1], and Shuting Li[1]

[1]Key Laboratory for Semi-Arid Climate Change of the Ministry of Education, College of Atmospheric Sciences, Lanzhou University, Lanzhou, China, [2]Collaborative Innovation Center for Western Ecological Safety, Lanzhou University, Lanzhou, China, [3]School of Atmospheric Sciences, and Key Laboratory of Tropical Atmosphere-Ocean System, Ministry of Education, Sun Yat-sen University, Zhuhai, China, [4]Southern Marine Science and Engineering Guangdong Laboratory, Zhuhai, China

Key Points:

- About one fourth of dust cases in East Asia from 2007 to 2020 originated from the Sahara Desert
- Long-range transported Saharan dust over East Asia was usually distributed in the upper troposphere where is >5 km above sea level
- Over East Asia, Saharan dust contributes 35.8% of total dust concentration in the upper troposphere in spring

Supporting Information:

Supporting Information may be found in the online version of this article.

Correspondence to:

Z. Huang and Z. Hu,
huangzhongwei@lzu.edu.cn;
huzhiyuan@mail.sysu.edu.cn

Citation:

Liu, Q., Huang, Z., Hu, Z., Dong, Q., & Li, S. (2022). Long-range transport and evolution of Saharan dust over East Asia from 2007 to 2020. *Journal of Geophysical Research: Atmospheres*, *127*, e2022JD036974. https://doi.org/10.1029/2022JD036974

Received 20 APR 2022
Accepted 30 AUG 2022

Author Contributions:

Conceptualization: Qiantao Liu, Zhongwei Huang
Data curation: Zhongwei Huang, Zhiyuan Hu, Qingqing Dong, Shuting Li
Formal analysis: Qiantao Liu, Zhiyuan Hu, Qingqing Dong, Shuting Li
Funding acquisition: Qiantao Liu, Zhongwei Huang
Investigation: Qiantao Liu, Zhongwei Huang
Methodology: Qiantao Liu, Zhongwei Huang, Zhiyuan Hu
Software: Qiantao Liu, Zhongwei Huang, Zhiyuan Hu
Supervision: Qiantao Liu, Zhongwei Huang
Writing – original draft: Qiantao Liu, Zhiyuan Hu
Writing – review & editing: Qiantao Liu, Zhongwei Huang, Zhiyuan Hu

Abstract Previous studies have shown that Saharan dust can be transported thousands of miles, affecting regional climates, environments, and ecosystems. However, research on the long-range transport of Saharan dust in Asia remains limited. We systematically investigated the long-range transportation of Saharan dust over East Asia from 2007 to 2020 using WRF-Chem model simulations, space-borne CALIPSO lidar observations, NCEP/NCAR reanalysis data, as well as HYSPLIT trajectory analysis. The results show that one quarter (24.3 ± 6.2%) of dust events in East Asia during 2007–2020 originated from the Sahara Desert. Moreover, long-range transported Saharan dust over East Asia was usually distributed in the upper troposphere. The average total amount of transported Saharan dust over East Asia between 2010 and 2015 was estimated at 33.05 ± 9.78 Tg/yr. Additionally, Saharan dust could be transported eastward all year and contributed about 35.8% of dust loading in the upper troposphere in Northern China in spring, which is almost the same amount of dust aerosols lifted up from East Asian dust sources. This study provides new sights on the important role of Saharan dust over East Asia, and elucidates the influence of long-range transported dust on regional climate and the water cycle.

1. Introduction

Saharan dust is the largest contributor to airborne dust (Tanaka & Chiba, 2006), accounting for about 57% of annual emissions of global dust (Huneeus et al., 2011; Ryder et al., 2019). Dust aerosols could directly affect the Earth-atmosphere system radiative budget by absorbing and scattering solar radiation (J. Huang et al., 2009; Mamun et al., 2021; Ryder et al., 2019), as well as indirectly by modifying cloud macro- and micro-properties by acting as active cloud condensation nuclei (CCN) (J. Huang et al., 2006; Karydis et al., 2011; Koehler et al., 2009) and heterogeneous ice nucleation particles (Hoose & Möhler, 2012; Sassen et al., 2003; Twohy et al., 2017) that affect cloud formation, and even influence precipitation (J. Huang et al., 2014). As light-absorbing particles (LAPs), Saharan dust affects radiative forcing and the water cycle by altering snow albedo (Dumont et al., 2020). The deposition of Saharan dust in the ocean also increases the carbon cycle of the ocean, as nutrients (Pabortsava et al., 2017). Through the Saharan heat low, dust also affects North African atmospheric dynamics and rainfall, hurricane development in North Atlantic (Colarco et al., 2014; Lavaysse et al., 2011; Pan et al., 2018; Ryder et al., 2019; Strong et al., 2018).

The uplift and long-range transport of Saharan dust is influenced by multi-scale weather systems. For example, an intense cyclone triggered by a northern Africa high altitude trough (Alpert & Ziv, 1989; Bou Karam et al., 2010), surface cold fronts (Knippertz & Todd, 2012) in Synoptic Scale, Mesoscale "haboob" (Emmel et al., 2010; Knippertz et al., 2007) and downward momentum transport due to early morning low-level jets (LLJs) (Allen & Washington, 2014; Caton Harrison et al., 2019). Furthermore, microscale dust devils can all trigger Saharan dust emissions (Ansmann et al., 2009; Koch & Renno, 2005). The very high atmospheric boundary layer of the Sahara Desert (usually reaching 5–6 km, considered the deepest on Earth, will contribute to lifting of Saharan dust to higher altitudes (Cuesta et al., 2020; Gamo, 1996). The presence of the African Eastern Jet (AEJ) at high altitude allows lifted dust transport westward to the Caribbean Sea (Thorncroft & Blackburn, 1999). Strong southwesterly airflow in front of an upper trough in North Africa allows for northward transport of lifting Saharan dust (Kutuzov et al., 2013). When strong zonal midtropospheric westerlies are present, lifted dust can be transported eastward through the westerlies (Hu, Huang, Zhao, Bi, et al., 2019; Hu et al., 2020). Merged with East Asian dust, Saharan dust can be further transported eastward to the Pacific Ocean after long-range transportion,

even reach and affect North America (McKendry et al., 2007). In transit across the Pacific Ocean, Saharan dust can interact with atmospheric rivers (Hu et al., 2022), causing precipitation and even flooding in western North America (Leung & Qian, 2009). Further, Creamean et al. (2013) observed that dust aerosols transported over long distances from the Sahara Desert are potential ice nucleation particles (INPs) in the western United States. Comparatively large amounts of Saharan dust are lifted by strong winds from the Sahara Desert and transported long distances along the tropical Atlantic Ocean to reach the Americas (Prospero, 1999; Prospero et al., 2014; Pu & Jin, 2021; Yu, Chin, Bian, et al., 2015; Yu, Chin, Yuan, et al., 2015; Yu et al., 2019). It is estimated that about 240 ± 80 Tg of dust which was transported from Sahara to the Atlantic Ocean using satellite observations annually (Kaufman et al., 2005). Additionally, Saharan dust transported to southwestern, western and central Europe has been observed, mainly above the boundary layer to 3–5 km, and even up to 7–8 km, above sea level (Ansmann et al., 2003). Consequently, Saharan dust was deposited in the European Alps, leading to an earlier snow melt date of 38 days (Di Mauro et al., 2019; Dumont et al., 2020). This transcontinental dust transport has already been investigated, and Uno et al. (2009) even verified that dust can circle the Earth.

Until now, most previous studies have proven that Saharan dust can be frequently transported westward through trade winds to the Atlantic Ocean and even to the Americas (Prospero et al., 1981) or northward to the Mediterranean (Bonasoni et al., 2004; Ganor & Mamane, 1982) through a cyclone (Perry et al., 1997). Only a few studies have noted its transport path eastward to East Asia. Ground-based lidar observations combined with multi-model simulations were used to verify that a dust event in East Asia in March 2005 was of Saharan origin (Bong Park et al., 2005). Combined multiple conventional observations with global aerosol transport model simulations, Tanaka et al. (2005) found that a dust event occurred in Japan on March 25–27, 2003 originated from the Sahara Desert and the Middle East, and mixed with pollutants during transportation, suggesting that the Sahara Desert may be an important source of dust over East Asia. Schlesinger et al. (2006) proved that Saharan dust have a significant impact on the microbial population in the air in the eastern Mediterranean, based on sampling analysis during four dust events in 2004 and 2005 in Haifa, Israel. Using observations and simulations, Hsu et al. (2012) showed that Saharan dust can be transported even further eastward to the North Pacific Ocean, contributing to over 50% of the overall dust deposition there. Zhang et al. (2017) confirmed that clouds and precipitation in East Asian coastal areas are mainly affected by Gobi, Sahara and Thar dust in spring combing satellite observations, reanalysis data as well as model simulation. The impact of dust on large-scale cloud and precipitation in the high latitudes of East Asian coastal areas becomes more intense. Therefore, the eastward Saharan dust also may have a noticeable impact on the weather, climate, environment and human health in East Asia. However, current research on the eastward transportation of Saharan dust is focused on the West Asia or coastal areas of East Asia by analyzing dust cases. Long-term characteristics and impact of the eastward transportation of Saharan dust is still lacking. Although Lee et al. (2006), modeling dust in 2000, found that Saharan dust could reach Japan within 9–10 days and generally had a higher impact on dust deposition there than East Asian dust. In terms of time scale, studies on the eastward transport of Saharan dust are still insufficient in a climatological view. Moreover, dust over East Asia is still widely believed to come from the Taklimakan Desert and Gobi Desert (Bong Park et al., 2005; Kurosaki & Mikami, 2007; Yumimoto et al., 2010).

Due to current lack of awareness of Sahara dust eastern transmission, we systematically described the characteristics of Saharan dust transported to East Asia by studying dust cases there in the past 14 years (2007–2020), and estimated the amount of dust transported, which can help to better understand its long-range transport characteristics and the sources of dust in East Asia, and further evaluate their impacts on climate and environment. In this study, CALIPSO lidar observations and WRF-Chem model simulations, combined with HYSPLIT and SPRINTARS models are applied to study the long-range transport of Saharan dust and evolution over East Asia from 2007 to 2020. Data and methods used are briefly described in Section 2, Section 3 includes the results and discussion, and conclusions are finally summarized in Section 4.

2. Data and Methods

2.1. CALIPSO Lidar Observation

The Cloud-Aerosol Lidar With Orthogonal Polarization (CALIOP) is a dual-wavelength (532 and 1,064 nm) polarized lidar on board the Cloud-Aerosol Lidar and Infrared Pathfinder Satellite Observation (CALIPSO) satellite (Winker et al., 2007; Yu et al., 2019). Its depolarization measurements can distinguish ice and water clouds, identifying non-spherical aerosol particles (J. Huang et al., 2007; Z. Huang et al., 2010; Winker et al., 2007).

The CALIOP can detect aerosol and cloud profiles, day and night, which are recorded with almost continuous high-resolution, since June 2006 (Ma et al., 2020; Winker et al., 2009, 2010). CALIOP's high resolution perpendicular profiling capability and precise depolarization measurements make it an excellent platform for studying dust aerosols (Liu, Liu, et al., 2008; Liu, Omar, et al., 2008; Z. Huang et al., 2022). In this study, the CALIPSO Level 1 product 532 nm total backscatter attenuation coefficient (version: 4.10) and Level 2 product vertical feature mask (VFM, version: 4.20) are used for identifying and tracking the dust layer.

2.2. NCEP/NCAR Reanalysis Data

Began in 1991, NCEP/NCAR reanalysis project produced past global analyses of atmospheric fields to feed the research requirements of climate monitoring communities (Chen & Liu, 2016; Kalnay et al., 1996; Kistler et al., 2001). Data assimilation based on a frozen state-of-the-art analysis/forecasting system using historical data from 1948 to the present (Chen & Liu, 2016; Kalnay et al., 1996). The quality and utility of the reanalysis data are effectively ensured by quality control, high vertical resolution, and the output of numerous meteorological fields (Z. Huang et al., 2015; Kalnay et al., 1996). The spatial resolution of the data is 2.5° × 2.5°, corresponding to a horizontal grid of 144 × 73 (Dell'Aquila et al., 2007). This study used daily atmospheric level geopotential height field data at 500 hPa to analyze Saharan dust long-range meteorological transport mechanisms in East Asian dust cases from 2007 to 2020.

2.3. HYSPLIT Trajectory Model

The HYSPLIT model, developed by the Air Resources Laboratory (ARL) of the National Oceanic and Atmospheric Administration (NOAA), is the most widely used model to analyze atmospheric transport and diffusion (Stein et al., 2015). The model can simulate transport and diffusion trajectories of various atmospheric pollutants. It is often used for backward trajectory analysis to ascertain the source of air masses (Fleming et al., 2012). The model calculation method combines Lagrangian and Eulerian methods. It is a relatively complete transfer, dispersion and deposition model with functions to handle the input domain of various meteorological elements as well as various physical procedures and different categories of pollutant emission sources. It is noted that the simulation of HYSPLIT backward trajectory has uncertainty, especially in the case of long-time simulation. Overall, the average trajectory error was about 15%–20% of the travel distance after a few days (Stohl, 1998). Therefore, trajectory analysis is usually only used as auxiliary evidence for tracing the source.

In this study, dust layer time, position and height were obtained by using CALIPSO level 2 VFM data. As the key model input information component, backward 240 hr simulation is carried out to obtain the dust transport path. The three-dimensional meteorological input for HYSPLIT was taken from the Global Data Assimilation System (GDAS) by NCEP/NCAR Reanalysis Project (Kanamitsu, 1989). The GDAS is run 4 times a day, that is, at 00, 06, 12, and 18 UTC. NCEP post-processing of the GDAS converts the data from spectral coefficient form to 1° latitude-longitude (360 by 181) grids and from sigma levels to mandatory pressure levels. In this study, the number of backward trajectories we analyzed is nearly 130,000.

2.4. WRF-Chem Model With Tracer Source Tagging

WRF-Chem is a new generation regional air quality model developed by NOAA Forecasting System Laboratory (FSL) in the United States. It is composed of the Weather Research and Forecasting (WRF) model and a chemistry component (Chem). During intercontinental transportation, a tracer-tagging method is used to label and clearly track dust particles (Hu, Huang, Zhao, Ma, et al., 2019). The WRF-Chem model with quasi-global simulation and tracer source tagging capability was utilized in this study (Hu et al., 2016; Hu, Huang, Zhao, Ma, 2019; Zhao, Chen, et al., 2013). The model contains 360 × 145 grid cells (67.5°S–77.5°N, 180°W–180°E), with a horizontal resolution of 1° × 1°, which are divided into 35 vertical layers (up to 50 hPa) (Hu, Huang, Zhao, Ma, et al., 2019). The North African Sahara Desert (0–40°N and 20°W–35°E), East Asia (25–50°N and 75–150°E), and the Middle East (0–50°N and 35–75°E) are used as dust sources to mark and clearly track dust particles from 2010 to 2015 (Hu, Huang, Zhao, Bi, et al., 2019; Hu, Huang, Zhao, Ma, et al., 2019; Mao et al., 2019). More detailed model setup information can be found in Zhao, Chen, et al. (2013) and Hu, Huang, Zhao, Bi, et al. (2019), and model simulation can be found in Hu et al. (2016) and Supporting Information S1. We used the model output results provided in Hu, Huang, Zhao, Ma, et al. (2019) to analyze specific characteristics of the eastward transport of Saharan dust and to calculate the amount of dust transported from the Sahara Desert to East Asia. Hu et al. (2020) showed that AOD simulated by WRF-Chem can be well represented in the spatial and seasonal variabilities

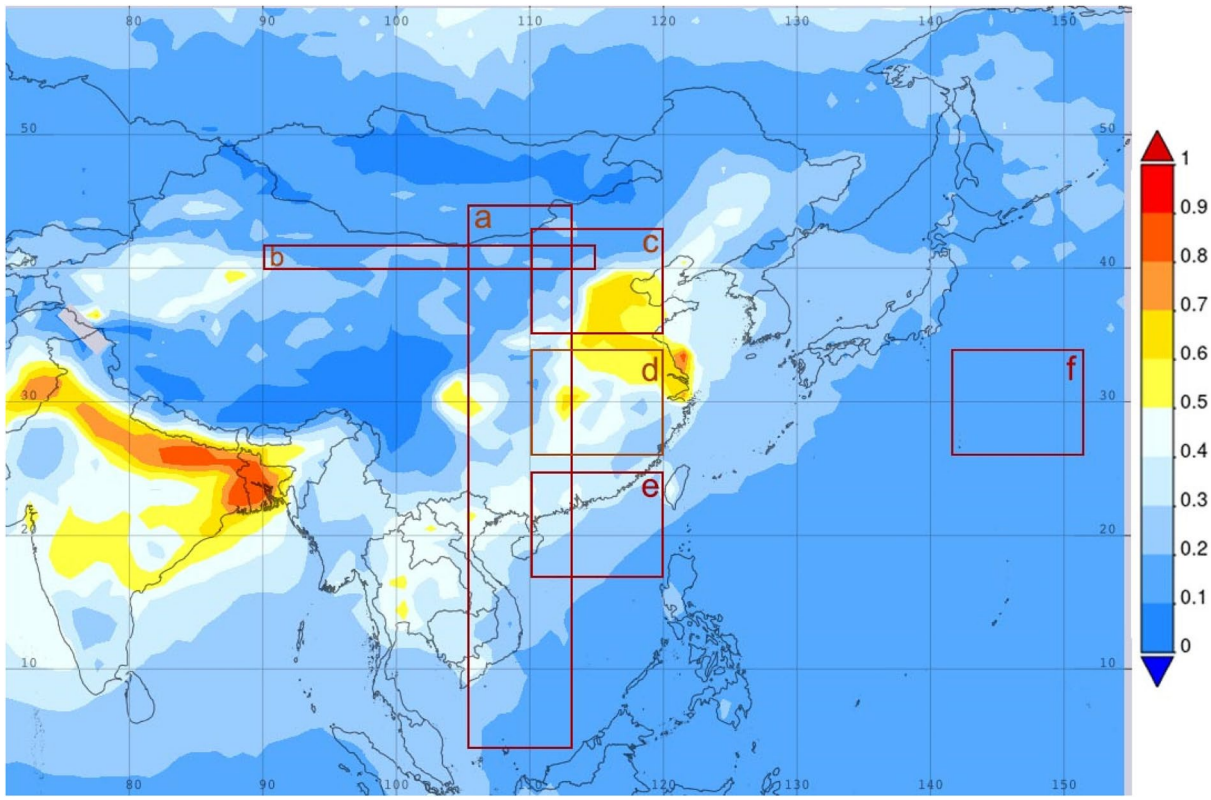

Figure 1. Distribution of averaged MODIS AOD at 550 nm over East Asia from 2020 to 2021. Region a–f (region a: 4°–45°N, 105°−113°E; region b: 40°−42°N, 90°−115°E; region c: 35°–43°N, 110°−120°E; region d: 26°−34°N, 110°−120°E; region e: 17°−25°N, 110°−120°E; region f: 26°−34°N, 142°−152°E) shows specific regions for detailed study.

comparing with results from MODIS and MISRobservation. In addition, the CALIPSO retrievals are used to compare the vertical profile of aerosol extinction, and results from simulation and observation are also consistent.

2.5. Dust Cases Identification

Six aerosol types were described in the vertical feature mask (VFM, version: 4.20) of CALIPSO Level 2 product, including clear marine, dust, polluted continental, clean continental, polluted dust, and smoke. Polarization measurement is very useful to distinguish dust from other aerosols (Z. Huang et al., 2018; Sugimoto & Huang, 2014), even dual-wavelength polarization can improve the identification of aerosol types (Dong et al., 2022; Z. Huang et al., 2020; Zhang et al., 2022). Among them, continuous dust and polluted dust were selected to identify the dust layer in region a (Figure 1). The selection reasons of specific region range can be seen in Section 3.1. If a dust layer appears in the region a, it is defined as a dust case. If dust layers in the study region lasted several consecutive days, they will be merged as a dust case.

We further can obtain detailed information on dust layer time, location and height was used as the key input information of HYSPLIT model, aiming to improve the reliability of model simulation (Z. Huang et al., 2015; Stein et al., 2009). The HYSPLIT model was used to conduct 240-hr backward trajectory simulation to see the transport pathway of dust aerosol (Chen et al., 2018). If the backward trajectory was traced to the Sahara Desert and confirmed by SPRINTARS model simulation, the dust case can be recognized as Saharan dust case. Finally, all Saharan dust cases were confirmed using CALIPSO lidar measurements from 2007 to 2020.

3. Results and Discussion

3.1. Saharan Dust Cases in East Asia

Generally, Saharan dust particles can be transported to East Asia via the westerlies (Hsu et al., 2012; Lee et al., 2006; Tanaka et al., 2005). Previous studies on long-range Saharan dust transport have mainly focused

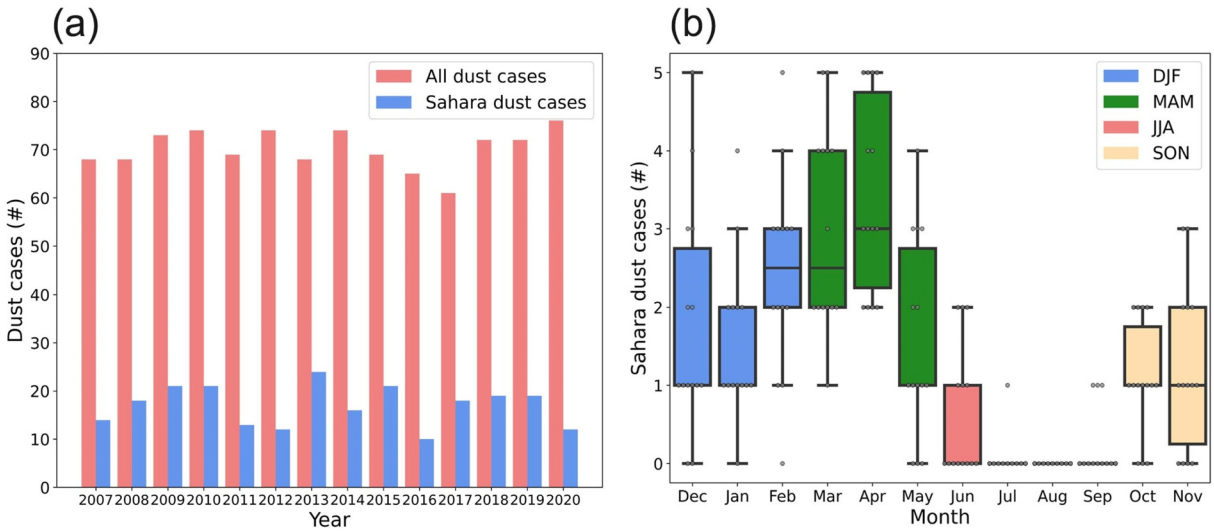

Figure 2. (a) All dust cases (red column) during 2007–2020 in region a (Figure 1), and dust cases that originated from the Sahara Desert (blue column) (b) Monthly averaged numbers of Sahara dust cases in East Asia. The line in the box indicates the median of all data arranged from smallest to largest, the upper and lower boundaries of the box indicate the first and third quartiles, respectively, and the lines at the top and bottom of the box indicate the upper and lower limits of the anomaly range, beyond which the data are considered outliers. The small dots in the figure indicate the number of specific cases in 14 years.

on individual cases, and so a climatological view of long-range transport is needed. To represent aerosol spatial characteristics, Figure 1 shows the distribution of averaged 550 nm AOD over East Asia observed by MODIS (https://giovanni.gsfc.nasa.gov/giovanni/). AOD values greatly vary spatially across China (Lee et al., 2007; Xin et al., 2007), although clearly, they are higher in coastal areas with a peak from 0.6 to 0.7, which is attributed to local pollution (Kim et al., 2007). Over the Taklimakan Desert, AOD reaches 0.5–0.6, which is mainly due to large amounts of dust (Sun et al., 2012).

In addition to anthropogenic emissions, high elevation is an important factor affecting dust transport. The Tibetan Plateau (TP) has an average altitude of 4,000 m, and can affect atmospheric circulation (Ding, 1992), even blocking dust transportation. To eliminate the influence of regional pollution and the TP topography on dust transport, we selected a long and narrow region to represent East Asia (region a in Figure 1). Here, we counted all dust cases over the past 14 years (2007–2020), and described long-range transport characteristics of Saharan dust to East Asia. According to the obtained dust transport path, we selected region b (Figure 1) to further study the distribution characteristics of eastward transported Saharan dust. Considering the dense population and frequent human activities in the eastern coastal area, the impact of dust may be more significant. Additionally, dust can also be deposited in the ocean as nutrients (Mills et al., 2004), which may also have important effects on the ocean. Therefore, we selected four small regions (c–f in Figure 1) and defined them as North China, Central China, South China and Western Pacific, respectively, to further analyze the vertical distribution of Saharan dust over East Asia.

Two hundred and thirty-eight (about 24.21%) of the 983 dust cases in region came from the Sahara Desert over the 14 years (2007–2020). There were more than 12 cases in 2020, accounting for 15.79%, and at most 24 in 2013, accounting for 35.29% (Figure 2a). Dust from the Sahara Desert accounts for almost a quarter of all dust cases in East Asia, showing that even deserts in distant regions cannot be ignored.

Dust cases from the Sahara Desert increased from January to April, from 1 to 3 on average (Figure 2b). From the beginning of May until September, the number of dust occurrences decreased, even dropping to none. This may be related to the Inter-tropical Convergence Zone (ITCZ) seasonal movement as one hemisphere warms relative to the other (Schneider et al., 2014), which will affect Saharan dust emission and transportation (Doherty et al., 2014). From a seasonal change perspective, four colors were used to represent the four seasons in the northern hemisphere (Figure 2b). In spring (green box), the highest number of cases of Saharan dust transported eastward were in April, which is well in agreement with previous global model simulations of Saharan dust by Lee et al. (2006). In spring (green box) there were on average about 3 Saharan dust cases in 14 years, followed by winter (blue box), with an average of about 2. The number in June was only 0–2, there was only one in July

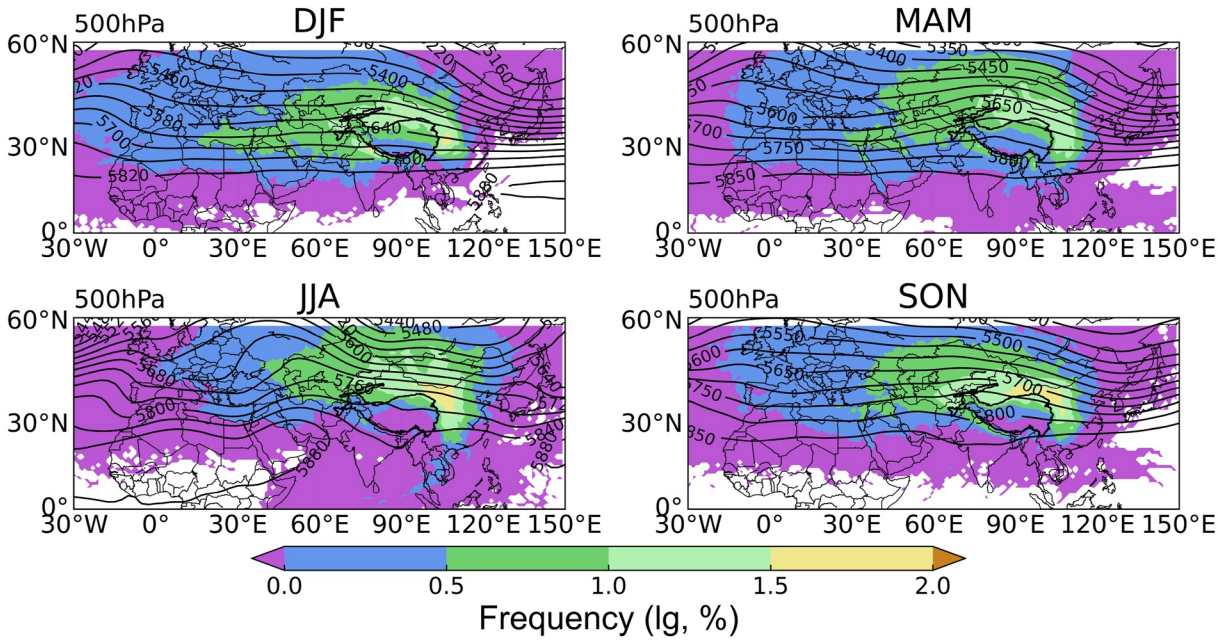

Figure 3. Long-range Saharan dust transport path derived from HYSPLIT backward trajectories analysis. The contour color represents the PDF distribution of 240-hr HYSPLIT backward trajectories for Saharan dust cases over East Asia, and the contour lines represent averaged geopotential height field at 500 hPa during dust cases from NCEP/NCAR reanalysis data.

(2011), and none in August over all 14 years. There was also one occurrence in September for 3 years, therefore, box plots were not drawn for any of the months of July to September due to so few Saharan dust cases. Such low dust case numbers in summer may be attributed to the northward shift of ITCZ (d'Almeida, 1986; Liu, Wang, et al., 2008) and the existence of easterly waves (Chen et al., 2018; Cuesta et al., 2020; Knippertz & Todd, 2012) that lead to the Sahara Desert area being mainly controlled by the Northeast air flow, whereby most of the dust moves westward to the Atlantic and America. Additionally, westerly belt weakening (Kuang & Zhang, 2005) and increased precipitation caused by the Asian summer monsoon (Ha et al., 2020) may weaken the eastward transport of dust during summer.

3.2. Long-Range Transport Path of Sahara Dust to East Asia

Saharan dust transport trajectories for all dust cases in 14 years were obtained by HYSPLIT model simulations. In the range 0°–60°N, 30°W–150°E, the probability density function (PDF) calculated as the ratio of the number of trajectories to the total trajectories appearing in each longitude and latitude grid (1° × 1°) (Z. Huang et al., 2015). The general path of Saharan dust transported eastward each year (PDF high value area) coincides with the 500 hPa geopotential height field (contours) distribution, and was determined from calculating PDFs annually (Figure 3). Because of the many and complex causes of Saharan dust uplift, we focus on how the uplifted Saharan dust is transported long distances to the east. According to Lee et al. (2006), using the global model and Chen et al. (2018) using a variety of aerosol measurement and reanalysis methods, lifted Saharan dust can reach an altitude of 650 hPa or 5 km above sea level, and be transported over long distance by high-altitude winds. This is also supported by the vertical distribution characteristics of North African dust observed by Liu, Wang, et al. (2008) using CALIPSO. Considering that the lifted dust can be transported over long distances through the westerly wind belt at high altitude (J. Huang et al., 2008; Uno et al., 2011), we chose only the 500 hPa geopotential height field to ascertain the general seasonal transport route of Saharan dust in relation to circulation. Since the front of the high-altitude trough generally corresponds to updraft, Saharan dust is generally lifted in front of the high altitude trough and transported eastward along the 500 hPa high altitude flow field (westerly wind belt) (Figure 3). Moreover, as stated by Lau and Kim (2006) and Hu, Huang, Zhao, Bi, et al. (2019), easterly transported Saharan dust is divide into north and south branches in the western part of the TP during transport, and reaches East Asia mainly through the northern branch. Dust in the southern branch, is mainly transported to the vicinity of the Himalayas. From the perspective of seasonal variation, the eastward transport path of Saharan dust in summer is more northerly than other seasonal paths. The reason may be that there is a high-pressure center

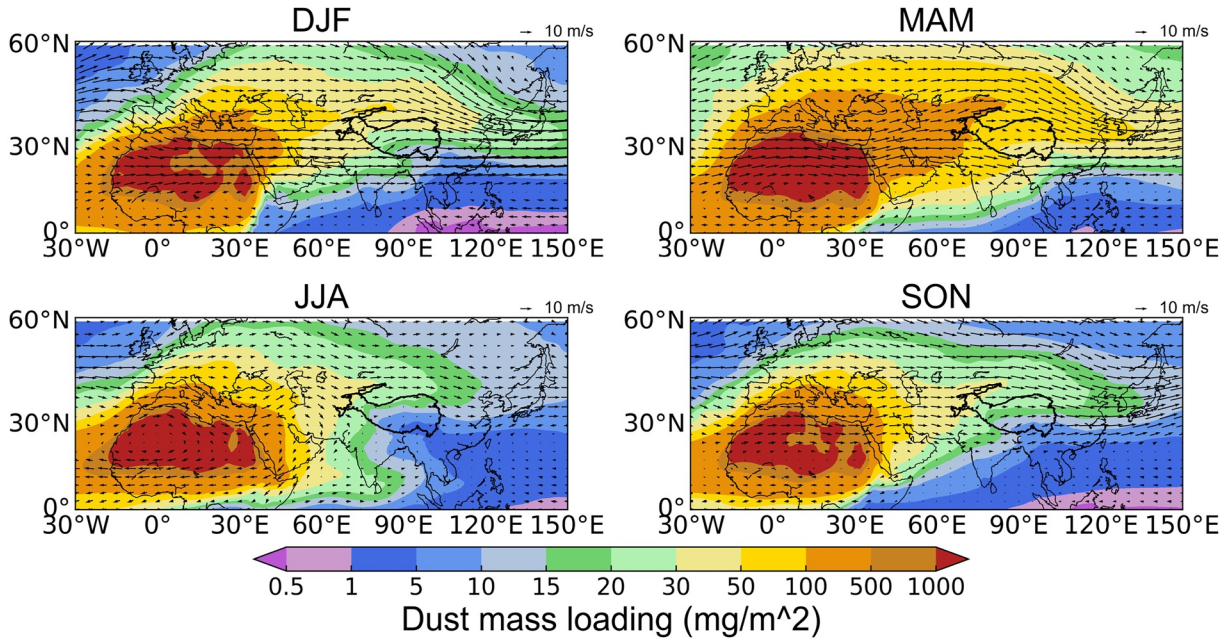

Figure 4. Spatial distributions of Saharan dust mass loading (mg/m^2) and wind field (m/s) at 500 hPa for four seasons during the period of 2010–2015, derived from WRF-Chem simulations.

in the south of Sahara Desert (Chen, 2005), which makes the high-altitude trough in the northwest of Sahara move northward, and the overall westerly belt moves northward. Our results show that Saharan dust can be transported directly from northern Africa to East Asia through the Mediterranean Sea, Caspian Sea and Central Asia in the whole year. Because the wind field is taken into account in the calculation of the trajectory, the randomness of turbulence leads to the inaccuracy of the calculation results (Stohl, 1998). Moreover, the origin of air parcels is not the same as the origin of particles, since a larger portion of particles are removed by wet or dry deposition during transportation (Yu et al., 2020). Therefore, this method of tracing the source by using the trajectory is usually verified in combination with different observations (such as satellite observations). For example, Uno et al. (2009) found that dust can travel around the world more than one full circuit around 13 days combing CALIPSO observation and HYSPLIT model simulation. So, we also further confirm transportation of dust using CALIPSO observation (Figures S1–S3 in Supporting Information S1, we take a dust case as an example).

To eliminate interference from other dust sources, the WRF-Chem model with tracer marker method was used for simulation and verification. Firstly, we verify the simulation results of the model for Saharan dust and further discuss seasonal differences in transport in the horizontal direction. We calculated the sum of the Saharan dust mass loading for all months within each season to more clearly reflect seasonal variation in the direction and amount of Saharan dust moving eastward. Since we only wanted to use the wind field (500 hPa) to determine Saharan dust transport, it was averaged over all months in a season and superimposed in Figure 4. High mass loading appeared in the Sahara Desert and there was almost no change in magnitude between seasons. Seasonal concentrations in East Asia were similar to in Figure 2b, with the highest in spring (MAM), between 50 and 100 mg/m^2, and least in summer (JJA), between 15 and 20 mg/m^2. Seasonal variation in Saharan dust eastern transportation was significant. During transportation of Saharan dust to East Asia, it meets the Tibetan Plateau and is divided into north and south branches. Except for in spring, the amount of dust transported through the north branch to East Asia is greater than through the south branch, due to the high topography of the Tibetan Plateau blocking and dust also being transported along the westerly wind belt. The south branch is concentrated in the Himalayas. This is consistent with the long-range transport trajectory of Saharan dust, as shown in Figure 3. In spring, westerly winds are strong, but they change significantly in summer, suggesting that dust transport is strongly influenced by changes in westerly wind belt intensity. Moreover, Saharan dust continues to be transported eastward to the ocean. In the spring maximum, 30–50 mg/m^2 are transported to the western Pacific, and in the summer minimum, only 10–15 mg/m^2 are transported. In the process of long-range eastern transportation, dust mass loading decreases, which is caused by continuous deposition during transportation. Overall, therefore, the accuracy of the model for Sahara dust simulation was demonstrated.

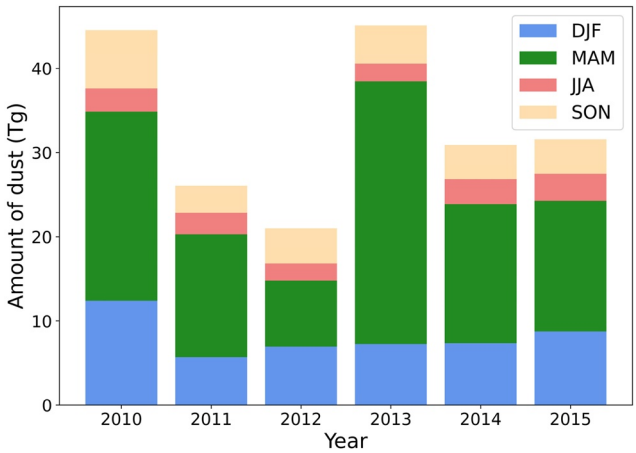

Figure 5. The amount (Tg) of Saharan dust in the atmosphere calculated by WRF-Chem simulation during 2010–2015.

In order to more accurately quantify the amount of dust transported from the Sahara to East Asia, we calculated the seasonal dust transport fluxes in four directions (east, west, south and north) in East Asia. The flux calculation formula, after Yu et al. (2008) and Hu, Huang, Zhao, Ma, et al. (2019), approximates the total amount of dust in the atmosphere transported from the Sahara to East Asia (Figure 5). Dust flux was greatest in spring, reaching 31.19 Tg in 2013, and lowest in 2012 at 7.86 Tg. The lowest dust flux mainly occurred in summer, with the highest of 3.22 Tg in 2015, and the lowest in 2012 at 2.02 Tg. Annual average dust transported from the Sahara Desert to East Asia was 33.05 Tg/yr, of which the minimum was 20.88 Tg in 2012, and the maximum was 44.94 Tg in 2013. In agreement with previous results, total dust transported from the Sahara was highest in spring with 18.02 Tg/yr and lowest in summer with 2.6 Tg/yr.

The model simulation results were further used to examine the horizontal distribution characteristics of Saharan dust eastward transport at different altitudes. Figure 6 shows the Saharan dust mass loading summed over all years, as in Figure 4. At 0–3 km above sea level, the model simulation results were blank because of high topography on the TP. The Sahara Desert had high values in all four seasons and the highest values in the Western Sahara region, reaching >1,000 mg/m^2. Other regions were also in the range of 500–1,000 mg/m^2, indicating that Saharan dust is active all year round (Knippertz & Todd, 2012). Furthermore, a large amount of Saharan dust (about 100–500 mg/m^2) is transported west over the four seasons. This is in agreement with previous understanding of the Saharan dust transport pathway (Liu, Wang, et al., 2008; Reid et al., 2002). The eastward transport of Saharan dust at 0–3 km is not very significant and is only 1–5 mg/m^2 in both summer and autumn. More Saharan dust in East Asia occurs near the Himalayas in the southern, rather than the northern part of the TP. In spring, Saharan dust over northern branch was 10–15 mg/m^2, while in the southern branch of the TP it was nearly twice as much, between 20 and 30 mg/m^2. Additionally, Saharan dust can still reach the western Pacific Ocean, and up to 10–15 mg/m^2 in spring.

At 3–5 km above sea level, the overall Saharan dust mass loading decreases, but it is still very active in spring and summer, with dust ranging from 100 to 500 mg/m^2 being lifted to very high altitude. Liu, Wang, et al. (2008) also found that in spring and summer the average height of the dust layer is about 4 km, further supporting our results. The amount transported eastward to the TP is 10–15 mg/m^2 in spring, 5–10 mg/m^2 in winter. Some Saharan dust enters the eastern TP, with 10–15 mg/m^2 in spring in the Qaidam Basin, about three times greater than the 1–5 mg/m^2 in all other seasons. When long-range transported Saharan dust enters the plateau, it affects the plateau climate and further influences downstream circulation and precipitation (Han et al., 2009). Dust from the Sahara will be further transported eastward to the western Pacific Ocean in amounts similar to those at 0–3 km.

At 5–7 km above sea level, 30–50 mg/m^2 of dust is present above the Sahara Desert in spring (Figure 7). Saharan dust is greatest in summer, at 50–100 mg/m^2, indicating that it is lifted higher in the summer, making long-range transportation possible (Uno et al., 2009). Meanwhile, Saharan dust can be seen over the entire TP, at 1–5 mg/m^2. At 7–12 km, although the east-borne Saharan dust is less than other altitudes, in East Asia in spring it reaches 5–10 mg/m^2. Dust at this altitude can act as an ice nucleus (IN), transforming supercooled water clouds into ice clouds and enhancing DCCs convective precipitation (Yin & Chen, 2007; Yuan et al., 2021). In general, the mass loading of Saharan dust is further reduced at elevations above 5 km, but it is mainly transported eastward and is most pronounced in spring. The dust transport path is also mainly alongside the northern branch path of the TP. In spring, at 5–7 and 7–12 km, the dust is mainly east-borne, while in summer, it is mainly west-borne. As mentioned, the Saharan dust can continue eastward to the western Pacific Ocean.

3.3. Vertical Distribution of Saharan Dust in East Asia

The eastern transmission of Saharan dust is mainly around 5 km above sea level (Figures 6 and 7), but we further analyzed its vertical distribution along the dust transport path. The eastward transportation of Saharan dust is mainly along the northern branch path to the north of the Tibetan Plateau (Figures 3, 4, 6 and 7). According to this general transportation path, we selected region b in Figure 1 to further analyze the vertical distribution characteristics of Saharan dust during transport along meridional and zonal directions. In order to further study the vertical distribution of Saharan dust in the South and North of East Asia, we extend the region b (40°–42°N,

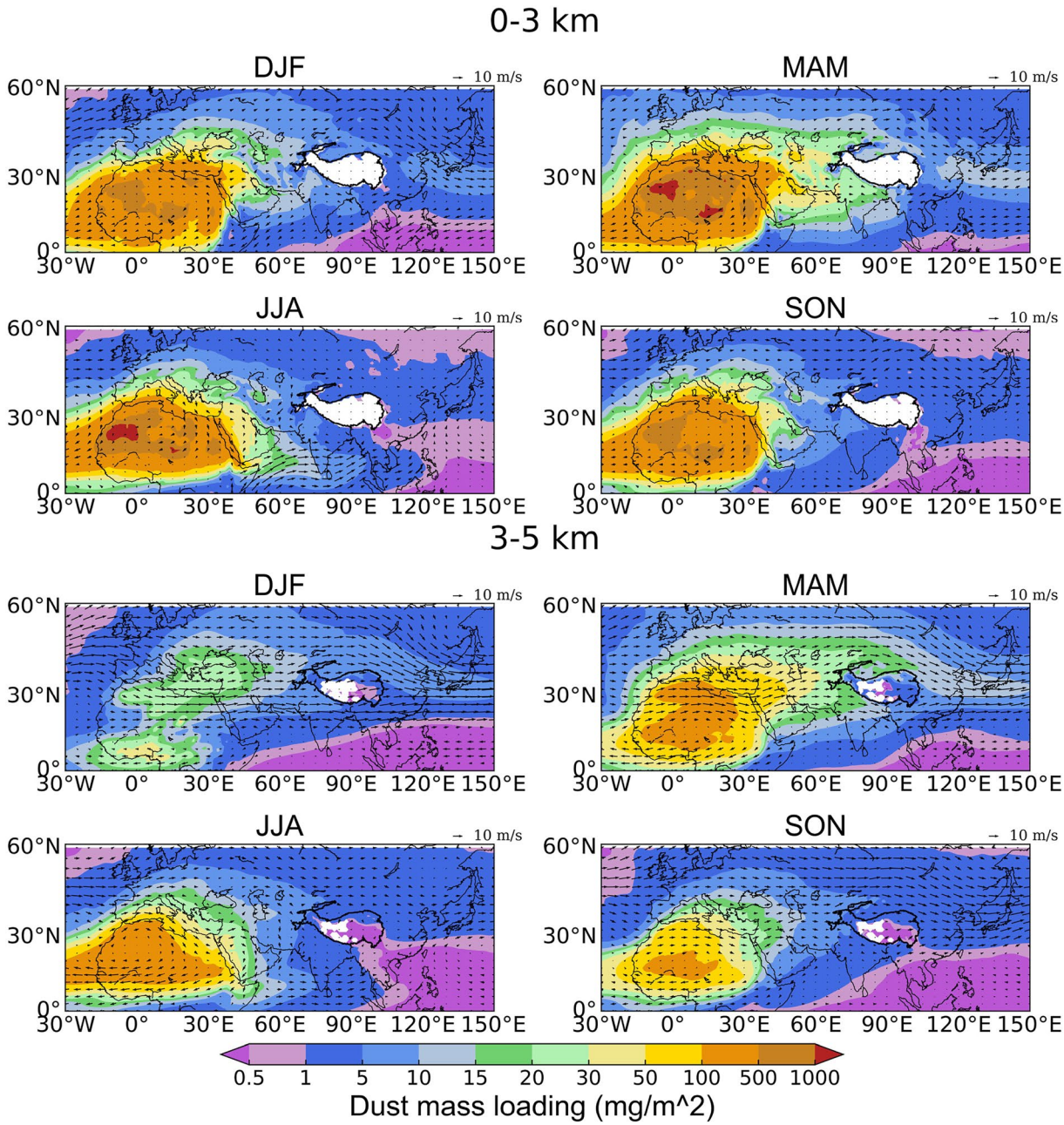

Figure 6. Spatial distributions of Saharan dust mass loading (mg/m^2) and average wind field (m/s) for four seasons at low- (0–3 km) and mid-altitude (3–5 km) in the troposphere.

90°−115°E) in Figure 1 in the meridional direction, that is, expand the region to 20°–50°N, 90°−115°E. To more clearly compare different Saharan dust concentrations over East Asia in different seasons, the model simulation results in Figure 8 were log-transformed. Saharan dust is transported in horizontal bands in four seasons. Similar to the results of Lee et al. (2006), the highest Saharan dust concentration was near 500 hPa (5.5 km above sea level), decreasing upward and downward, and it was the highest in spring (Figures 2b and 4). The whole Saharan dust covers a wide range over East Asia in spring, from 30 to 50°N, and from the ground to high altitude. Surface Saharan dust concentration around 40°N is 0.4 μg/m^3, while at 30°N, it is >0.1 μg/m^3. Above 700 hPa (3 km above sea level), it ranges from 20° to 50°N, and can reach 0.8 μg/m^3 at 40°N. In winter and spring, Saharan dust is not only concentrated in northern China, but also present at high altitudes in southern China (south of 30°N). This is consistent with the results in Figure 7. Similarly, in winter, Saharan dust of 0.1 μg/m^3 can still be seen

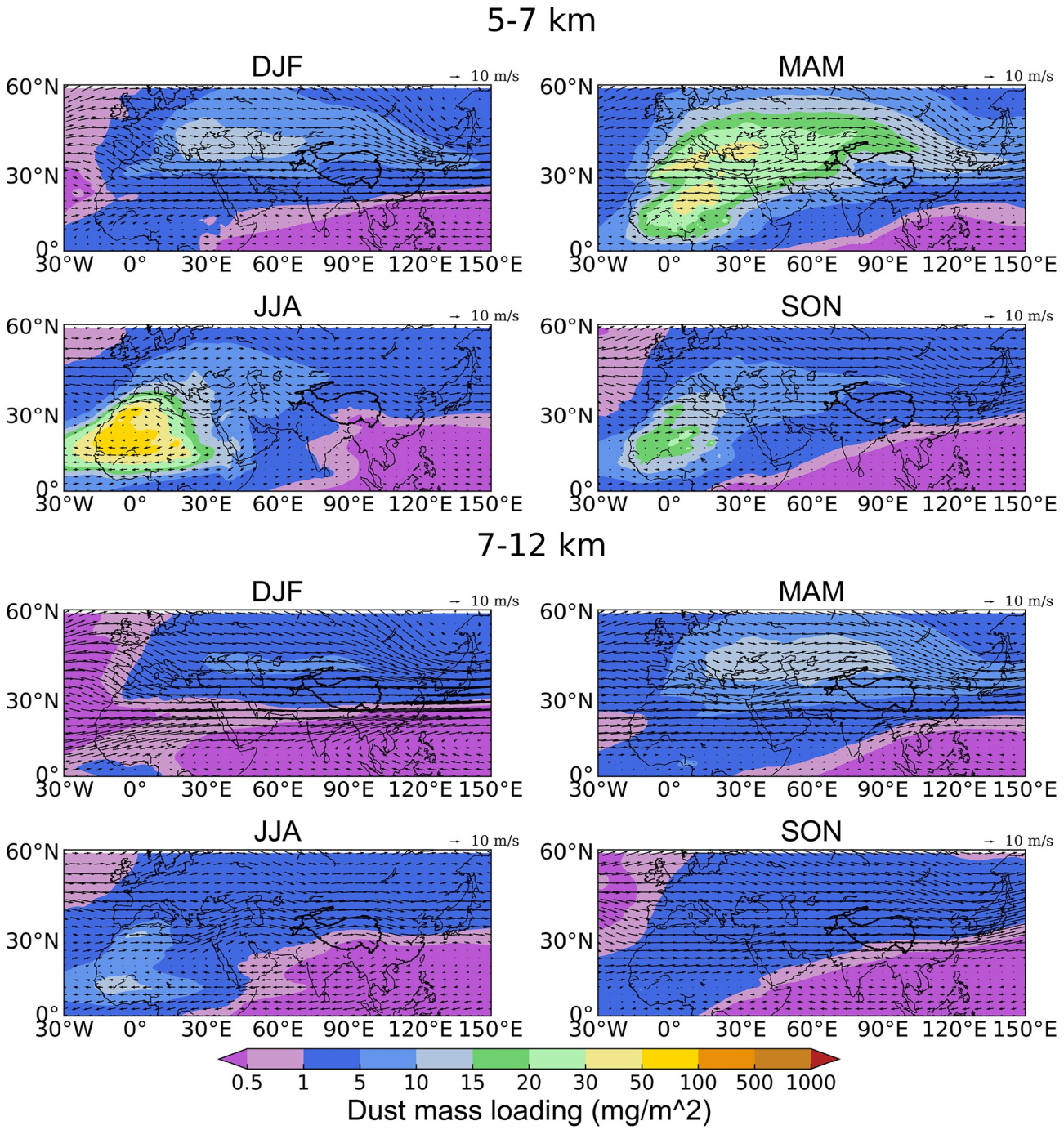

Figure 7. Spatial distributions of Saharan dust mass loading (mg/m^2) and average wind field (m/s) for four seasons for high altitudes (5–7 km and 7–12 km).

at 700–500 hPa south of 30°N. Thus, Saharan dust has a wide impact in East Asia. In summer, the Saharan dust concentration position moves northward and is concentrated between 40 and 50°N, which is coincide with the higher concentration of Saharan dust at 5–7 km in summer rather than spring in Figure 7, where it is lifted to higher altitudes, as it travels eastward to East Asia.

A similar altitude and seasonal distribution can be seen in Figure 9, and so Saharan dust concentrations we likewise log-transformed. Saharan dust is transported to East Asia in the form of belt, and concentrated near 500 hPa, decreasing upward and downward. In spring Saharan dust concentration is the highest, more than 0.9 μg/m^3, and in summer it is the lowest, at 0.2 μg/m^3. Additionally, concentration of Saharan dust decreases along its transport

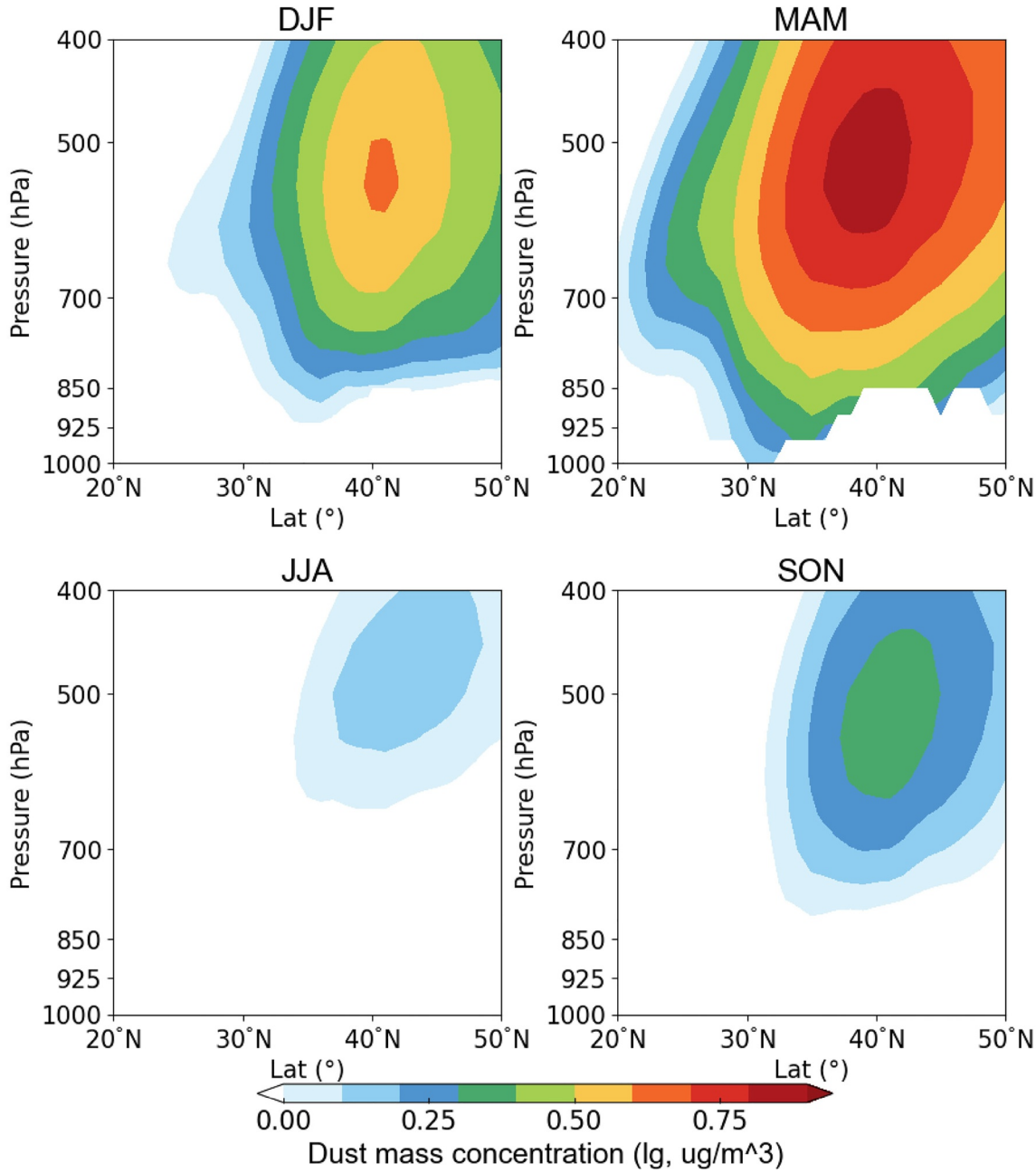

Figure 8. Vertical cross-sections of meridional dust mass concentration (μg/m^3) originating from the Sahara Desert in different seasons from the WRF-Chem model simulation during 2010–2015 (in region 20°–50°N, 90° − 115°E).

path. The highest Saharan dust concentration area also decreases in height, and a large amount of dust can be found on the windward slope of the mountains. In spring, 0.8–0.9 μg/m^3 of dust appeared on the top of the windward slope, and in summer it was the least, at nearly 0.1 μg/m^3. If the Saharan dust settles on the windward slope of the mountains, it can affect snow cover, hydrological changes and ecology (Sarangi et al., 2020). Saharan dust concentration in the upper air also changes due to the influence of terrain ranging from 95 to 100°E. Additionally, in summer, the extension of Saharan dust in the vertical range east of 105°E is significantly less than in other seasons, and the concentration height is also above 500 hPa, which is consistent with greater height of Saharan dust in summer (Figures 7 and 8).

Saharan dust is mainly concentrated in the upper air of East Asia, and its effects are widespread, and will appear in the upper air of southern China. Therefore, we selected four different regions (regions c–f in Figure 1) to observe

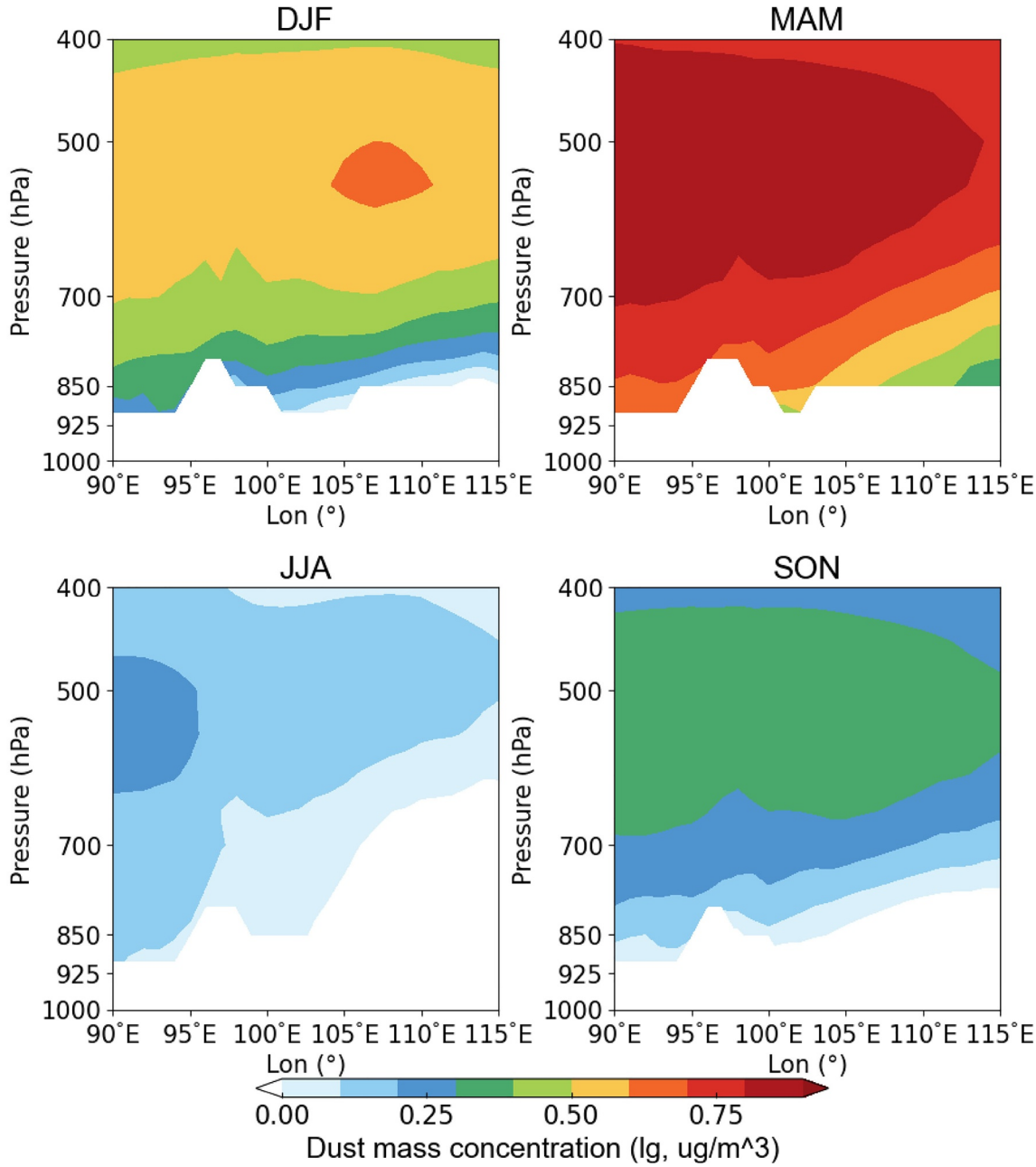

Figure 9. Vertical cross-sections of zonal dust mass concentration (μg/m^3) originating from the Sahara Desert in different seasons from the WRF-Chem model simulation during 2010–2015 (in region 40°–42°N, 90°−115°E).

Saharan dust vertical distribution. Additionally, since the WRF-Chem model can simulate the dust distribution of different dust sources (Sahara, Central Asia and East Asia), we can examine differences between Saharan dust and other dust sources. Figure 10 shows the dust concentration profiles of different dust sources in regions c and d in different seasons obtained from the WRF-Chem model. To reduce the magnitude of difference between different dust sources, we log-transformed all concentrations. In North China and Central China, long-range transport of Saharan dust caused similarly vertical distributions, both initially increasing and then decreasing with increasing height, with high concentration at 500 hPa. East Asian dust was mainly concentrated at low altitudes, and its dust concentration decreased with increasing height. Below 500 hPa, the East Asia dust concentration was almost twice that of Sahara and Central Asia dust. Therefore, East Asia dust will affect human activities more (Yin et al., 2021). However, above 500 hPa in spring, the three dust concentrations were nearly equivalent. At the

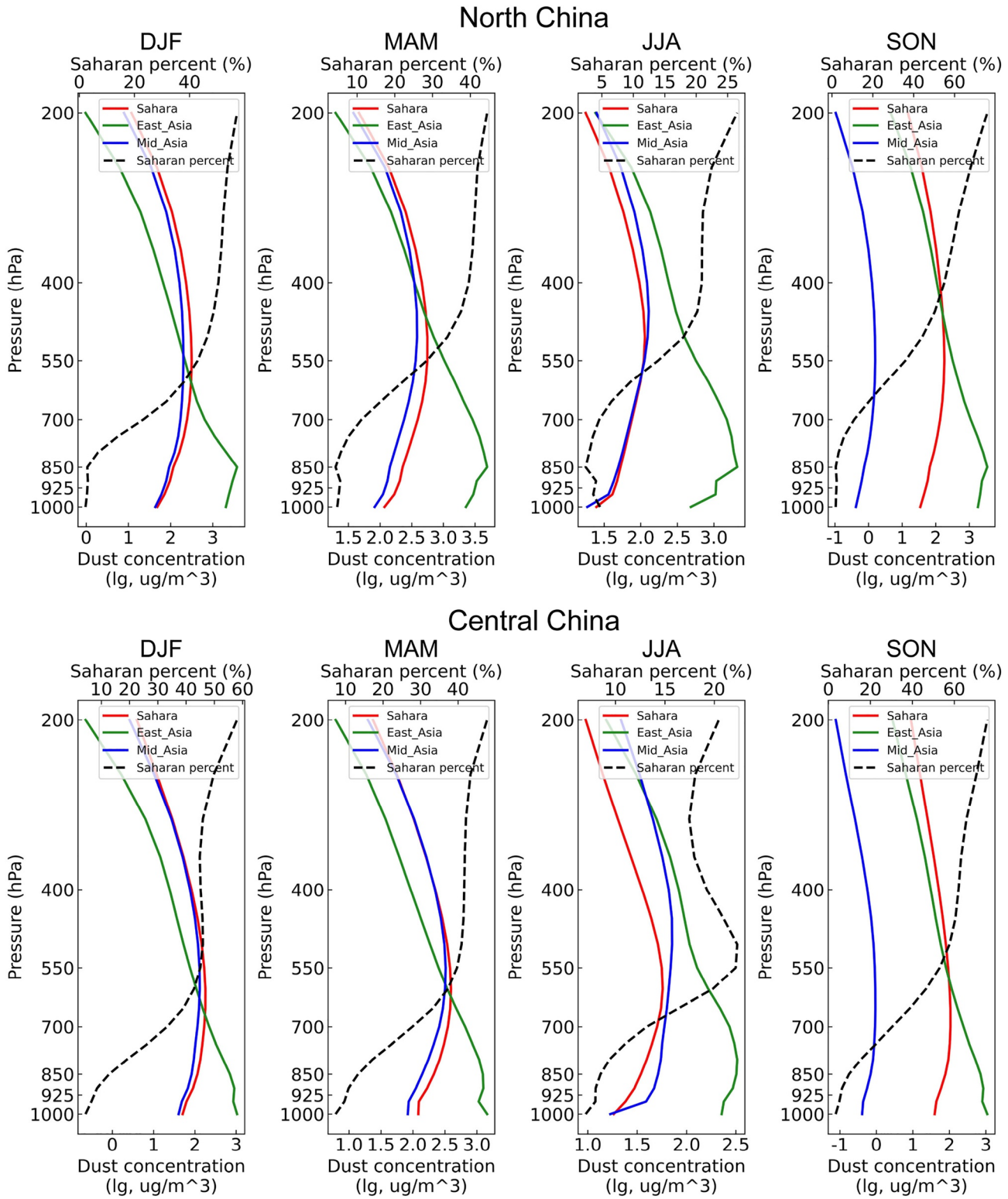

Figure 10. Vertical distribution of Sahara dust concentration from different dust sources in North and Central China in different seasons from 2010 to 2015 simulated by WRF-Chem.

same time, above 400 hPa, except in summer, the Saharan dust concentration in other seasons was the greatest of all three kinds of dust. This pattern also showed from the proportion of Saharan dust in the three dust types (black dotted line). The proportion of Saharan dust increased from 850 hPa and remained almost unchanged above 400 hPa. In autumn and winter, Saharan dust accounted for nearly 50% above 400 hPa, while it was 40% in spring and 20% in summer. The higher the altitude, the greater the proportion of Saharan dust, and so its role cannot be ignored, as it may further affect high-altitude cirrus clouds and thus precipitation (Creamean et al., 2013; Twohy et al., 2017). In Central China, dust concentration and magnitudes in different dust sources were similar to in North China, but in spring and summer, all dust concentrations above 500 hPa were lower, indicating less Saharan dust reaching the upper air in Central China. In summer, the proportion of Saharan dust initially increases with height, decreases after 500 hPa, and increases again after 400 hPa. This is not only related to the sharp reduction of Saharan dust itself at high altitude, but also related to the sharp reduction of East Asian dust above 400 hPa.

Figure 11 shows the distribution of dust concentrations in regions e and f (Figure 1) obtained from the WRF-Chem model for different seasons and different dust source areas. In South China, the dust concentration increases initially, and then decreases with height, but the maximum concentration decreases, and is lower than 550 hPa. The overall dust concentration is lower than in North and Central China, and in winter and spring, there is little difference in dust concentration between different dust sources below 850 hPa. But above 400 hPa, Saharan dust still accounts for 50%–60% as in North and Central China, which shows that Saharan dust will also have an impact on South China. In summer, the proportion of Saharan dust concentration above 400 hPa decreases to about 16%. In contrast to North and Central China, the East Asia dust concentration is lower than for Central Asia at all heights, the minimum concentration is below 850 hPa, and there is no change with height, indicating that East Asia dust has a weak impact on South China. The ratio of dust initially increased, and then decreased from 550 hPa. In the Western Pacific, the overall change trend is similar to that in South China, but in spring, the proportion of Saharan dust above 400 hPa is between 40% and 45%, which is lower than in the first three regions. Concurrently, the maximum value for all dust types occurred at 700–550 hPa, which is lower than the first three areas. This is most likely due to inevitable dust settlement during transportation. The proportion of Saharan dust concentrated above 400 hPa increased significantly, and increased by 10%–20% in different seasons. Although Saharan dust concentration in the Western Pacific decreases and the main height decreases, its importance above 400 hPa cannot be ignored.

As Saharan dust is mainly concentrated at high altitudes (above 5 km above sea level; see Figures 8–11), we focused on the dust concentrations and proportions of different dust sources >5 km above sea level in the four selected study areas. Overall dust concentrations are the least in South China and the most in North China (Figure 12), and in spring North China has the highest dust concentration of 88.33 $\mu g/m^3$. The dust in the upper air of South China is the least, and is highest in spring, where the dust above 5 km is 7.92 $\mu g/m^3$. Dust concentration in high air decreases from north to south in China (Figure 12). Although the latitude of the Western Pacific is the same as Central China, dust concentration in the upper air is lower because it is farther away from the dust source. East Asian dust activity is also most frequent in North China in spring (Tian et al., 2020), so the proportion of East Asian dust is highest then, and in summer can reach 58.1%. But the proportion of Saharan dust is comparable to that of East Asian dust, for example, in spring in North China, East Asian dust accounts for 37.7% and Saharan dust accounts for 35.8%. Except for summer, all regions are dominated by East Asian dust, and all other seasons are dominated by Saharan dust. The highest proportion of Saharan dust is 48.6%, which occurs in spring in South China. Using a global dust transport model, Tanaka and Chiba (2006) simulated an atmospheric load of about 1.1 Tg in East Asia (Eastern and Western China). Moreover, in East Asia, Saharan dust accounts for 20% to more than 30% of the annual dust load, and Arabian dust accounts for 10%. Therefore, the role of Saharan dust in East Asia cannot be ignored. Its radiative and indirect effects will further affect clouds, atmospheric circulation and East Asian monsoon, affecting precipitation, and thus the water cycle system in East Asia and even the whole world.

4. Conclusions

To better understand long-range transport of Saharan dust, we investigate its transport path and dust aerosol populations in East Asia combined satellite observation, model simulations as well as reanalysis data. Firstly, we selected all dust cases in East Asia during 2007–2020 from CALIPSO lidar observations, and then validated by HYSPLIT trajectory and SPRINTARS models. Secondly, we examined Saharan dust long-range transport paths

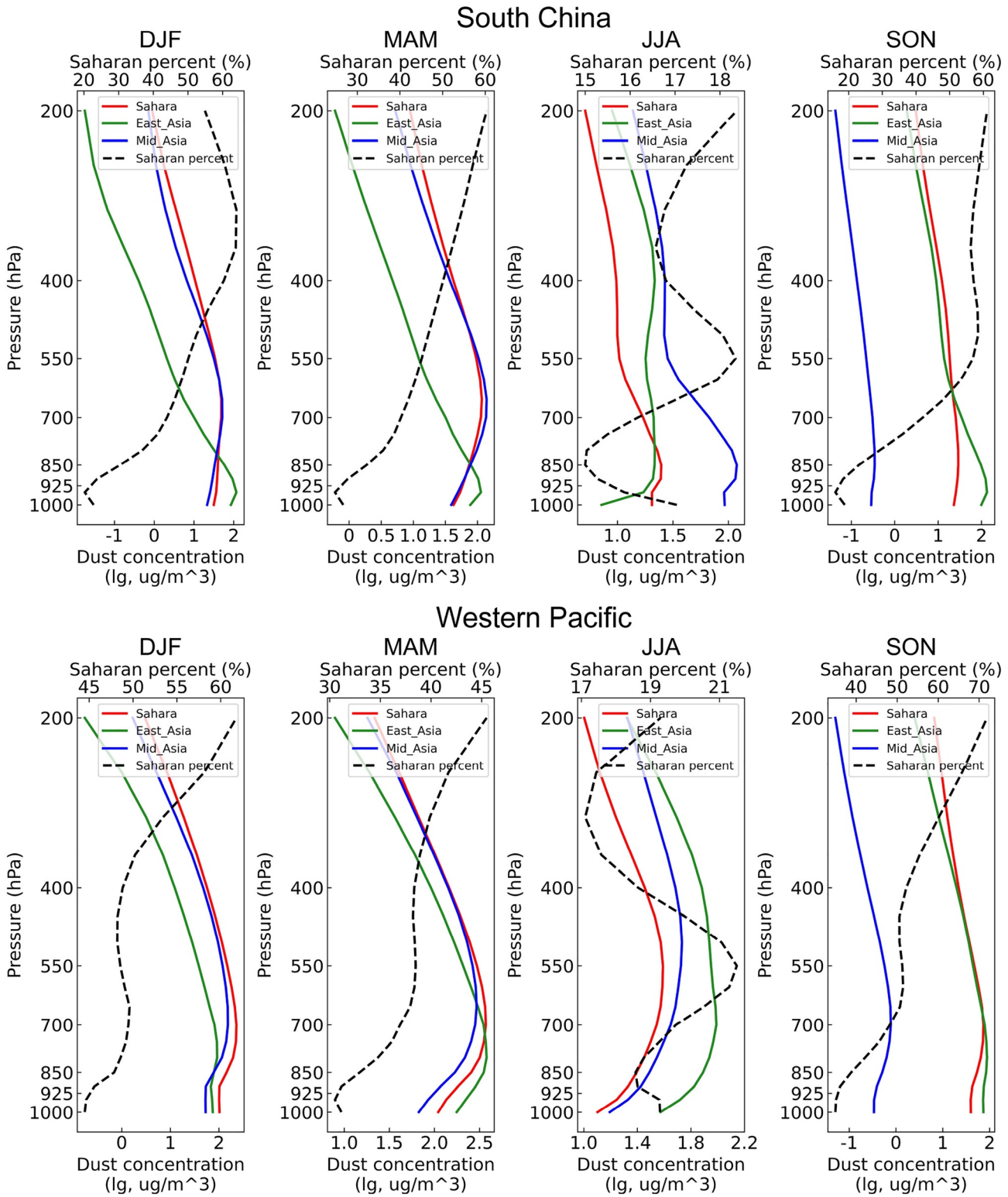

Figure 11. Vertical distribution of Sahara dust concentration from different dust sources in South China and Western Pacific in different seasons from 2010 to 2015 simulated by WRF-Chem.

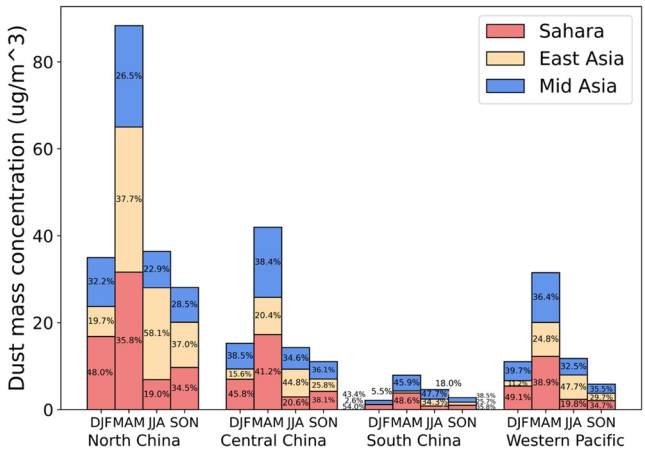

Figure 12. Mass concentration of dust aerosols originated from the Sahara Desert, Middle Asia and East Asia at high-altitude (5 km) obtained from the WRF-Chem simulation for four regions over East Asia during the period 2010–2015.

using models and NCEP/NCAR reanalysis data. Finally, we investigated Saharan dust distribution in East Asia based on WRF-Chem simulation.

We found that 24.3 ± 6.2% of dust cases in East Asia during 2007–2020 originated from the Sahara Desert, at least 12 times in 2020, accounting for 15.79%, and the most 24 times in 2013, accounting for 35.29%. Dust from the Sahara Desert accounted for almost a quarter of all dust cases in East Asia, demonstrating that even deserts in distant regions cannot be ignored. Seasonal variation in the eastern transportation of Saharan dust is significant. In spring, the most cases of Saharan dust transported eastward were concentrated in April, with an average of about 3 times in 14 years, followed by winter, with an average of about twice in 14 years. It is similar with results by Lee et al. (2010), suggesting that Hong Kong was most affected by dust from East Asia and other distant desert in March, but not in summer. Saharan dust could be transported eastward in all seasons, and mainly located in the high altitude westerly airflows. Easterly-transported Saharan dust divides into north and south branches during the transport process, and reaches East Asia mainly through the northern branch. However, from a year-by-year perspective, the Saharan dust transport path does not show a trend of movement to the south or north, this may only reflect the limited time frame of our study.

The amount of Saharan dust in East Asia estimated by our WRF-Chem model was 33.05 ± 9.78 Tg/yr, and was highest in spring and lowest in summer. Eastern transmission of Saharan dust is mainly around 5 km above sea level. In spring, the whole Saharan dust covers a wide range over East Asia. In both winter and spring, Saharan dust is not only concentrated in the northern part of China, but also present at high altitudes in southern China (south of 30°N). Moreover, the higher the altitude, the greater the proportion of Saharan dust among all dust origins. Its role cannot be ignored, which may further affect high-altitude cirrus clouds and thus precipitation. In spring, Saharan dust contributed 35.8% of dust loading to the upper troposphere in North China, which is almost the amount of dust aerosols lifted up from East Asian dust sources. This brings to light the important role of Saharan dust in East Asia. Quantitative analysis of the amount of long-range transported Saharan dust is very useful to better evaluate the impact of dust on climate and environment over east Asia. However, the WRF-Chem model simulation was not long enough for us to investigate variation of the dust transported from Sahara Desert to East Asia on longer time scales. Furthermore, the effects of Saharan dust as ice nuclei on precipitation in East Asia and as absorbing particles deposited on snow and glaciers in East Asia could not be addressed. These are important issues in East Asia and will be investigated in future.

Data Availability Statement

The CALIPSO lidar observation data are freely available from Atmospheric Science Data Center (NSDC) website (https://subset.larc.nasa.gov/calipso/). You need to register before downloading data. The NCEP/NCAR reanalysis data (Kalnay et al., 1996) was obtained from NOAA Physical Sciences Laboratory website (https://psl.noaa.gov/thredds/catalog/Datasets/ncep.reanalysis/catalog.html). The installation of HYSPLIT trajectory model PC version is downloaded from NOAA Air Resources Laboratory website (https://www.ready.noaa.gov/documents/Tutorial/html/index.html). HYSPLIT model (Rolph et al., 2017; Stein et al., 2015) also can run online from NOAA Air Resources Laboratory website (https://www.ready.noaa.gov/HYSPLIT_traj.php). The updated version of WRF-Chem model is available by downloading from https://doi.org/10.5281/zenodo.4663508 (last access: 17 March 2022) (Zhao & Zhang, 2021). The MODIS AOD products were obtained from NASA's Giovanni project website (https://giovanni.gsfc.nasa.gov/giovanni/). In this web page, you can automatically generate figures by selecting datasets.

Acknowledgments
This research was funded by the Second Tibetan Plateau Scientific Expedition and Research Program (STEP), Grant No. 2019QZKK0602, National Natural Science Foundation of China (41875029, 42015705); Higher Education Discipline Innovation Project–111 Project (B 13045); the Project of Field Scientific Observation and Research Station of Gansu Province (18JR2RA013); We are grateful to the CALIPSO (https://eosweb.larc.nasa.gov/) science team for providing CALIPSO data. We also thank Prof. Toshihiko Takemura at Research Institute for Applied Mechanics, Kyushu University for providing SPRINTARS model data (https://sprintars.riam.kyushu-u.ac.jp/archive.html). NCEP reanalysis data are provided by the NOAA/OAR/ESRL PSD (http://www.esrl.noaa.gov). Air mass trajectories were reconstructed using the NOAA ARL website (http://ready.arl.noaa.gov).

References

Allen, C. J. T., & Washington, R. (2014). The low-level jet dust emission mechanism in the central Sahara: Observations from Bordj-Badji Mokhtar during the June 2011 Fennec intensive observation period. *Journal of Geophysical Research: Atmospheres*, *119*(6), 2990–3015. https://doi.org/10.1002/2013JD020594

Alpert, P., & Ziv, B. (1989). The Sharav cyclone: Observations and some theoretical considerations. *Journal of Geophysical Research*, *94*(D15), 18495–18514. https://doi.org/10.1029/JD094iD15p18495

Ansmann, A., Bösenberg, J., Chaikovsky, A., Comerón, A., Eckhardt, S., Eixmann, R., et al. (2003). Long-range transport of Saharan dust to northern Europe: The 11–16 October 2001 outbreak observed with EARLINET. *Journal of Geophysical Research*, *108*(D24). https://doi.org/10.1029/2003JD003757

Ansmann, A., Tesche, M., Knippertz, P., Bierwirth, E., Althausen, D., Müller, D., & Schulz, O. (2009). Vertical profiling of convective dust plumes in southern Morocco during SAMUM. *Tellus B: Chemical and Physical Meteorology*, *61*(1), 340–353. https://doi.org/10.1111/j.1600-0889.2008.00384.x

Bonasoni, P., Cristofanelli, P., Calzolari, F., Bonafè, U., Evangelisti, F., Stohl, A., et al. (2004). Aerosol-ozone correlations during dust transport episodes. *Atmospheric Chemistry and Physics*, *4*(5), 1201–1215. https://doi.org/10.5194/acp-4-1201-2004

Bong Park, C., Sugimoto, N., Matsui, I., Shimizu, A., Tatarov, B., Kamei, A., et al. (2005). Long-range transport of Saharan dust to East Asia observed with lidars. *SOLA*, *1*, 121–124. https://doi.org/10.2151/sola.2005-032

Bou Karam, D., Flamant, C., Cuesta, J., Pelon, J., & Williams, E. (2010). Dust emission and transport associated with a Saharan depression: February 2007 case. *Journal of Geophysical Research*, *115*(D4), D00H27. https://doi.org/10.1029/2009JD012390

Caton Harrison, T., Washington, R., & Engelstaedter, S. (2019). A 14-year climatology of Saharan dust emission mechanisms inferred from automatically tracked plumes. *Journal of Geophysical Research: Atmospheres*, *124*(16), 9665–9690. https://doi.org/10.1029/2019JD030291

Chen, B., & Liu, Z. (2016). Global water vapor variability and trend from the latest 36 year (1979 to 2014) data of ECMWF and NCEP reanalyses, radiosonde, GPS, and microwave satellite. *Journal of Geophysical Research: Atmospheres*, *121*(19), 11442–11462. https://doi.org/10.1002/2016JD024917

Chen, S.-P., Lu, C.-H., McQueen, J., & Lee, P. (2018). Application of satellite observations in conjunction with aerosol reanalysis to characterize long-range transport of African and Asian dust on air quality in the contiguous U.S. *Atmospheric Environment*, *187*, 174–195. https://doi.org/10.1016/j.atmosenv.2018.05.038

Chen, T.-C. (2005). Maintenance of the midtropospheric North African summer circulation: Saharan high and African easterly jet. *Journal of Climate*, *18*(15), 2943–2962. https://doi.org/10.1175/JCLI3446.1

Colarco, P. R., Nowottnick, E. P., Randles, C. A., Yi, B., Yang, P., Kim, K.-M., et al. (2014). Impact of radiatively interactive dust aerosols in the NASA GEOS-5 climate model: Sensitivity to dust particle shape and refractive index. *Journal of Geophysical Research: Atmospheres*, *119*(2), 753–786. https://doi.org/10.1002/2013JD020046

Creamean, J. M., Suski Kaitlyn, J., Rosenfeld, D., Cazorla, A., DeMott Paul, J., Sullivan Ryan, C., et al. (2013). Dust and biological aerosols from the Sahara and Asia influence precipitation in the Western U.S. *Science*, *339*(6127), 1572–1578. https://doi.org/10.1126/science.1227279

Cuesta, J., Flamant, C., Gaetani, M., Knippertz, P., Fink, A. H., Chazette, P., et al. (2020). Three-dimensional pathways of dust over the Sahara during summer 2011 as revealed by new infrared atmospheric sounding interferometer observations. *Quarterly Journal of the Royal Meteorological Society*, *146*(731), 2731–2755. https://doi.org/10.1002/qj.3814

d'Almeida, G. A. (1986). A model for Saharan dust transport. *Journal of Applied Meteorology and Climatology*, *25*(7), 903–916. https://doi.org/10.1175/1520-0450(1986)025<0903:Amfsdt>2.0.Co;2

Dell'Aquila, A., Ruti, P. M., Calmanti, S., & Lucarini, V. (2007). Southern Hemisphere midlatitude atmospheric variability of the NCEP-NCAR and ECMWF reanalyses. *Journal of Geophysical Research*, *112*(D8), D08106. https://doi.org/10.1029/2006JD007376

Di Mauro, B., Garzonio, R., Rossini, M., Filippa, G., Pogliotti, P., Galvagno, M., et al. (2019). Saharan dust events in the European Alps: Role in snowmelt and geochemical characterization. *The Cryosphere*, *13*(4), 1147–1165. https://doi.org/10.5194/tc-13-1147-2019

Ding, Y. (1992). Effects of the Qinghai-Xizang (Tibetan) plateau on the circulation features over the plateau and its surrounding areas. *Advances in Atmospheric Sciences*, *9*(1), 112–130. https://doi.org/10.1007/BF02656935

Doherty, O. M., Riemer, N., & Hameed, S. (2014). Role of the convergence zone over West Africa in controlling Saharan mineral dust load and transport in the boreal summer. *Tellus B: Chemical and Physical Meteorology*, *66*(1), 23191. https://doi.org/10.3402/tellusb.v66.23191

Dong, Q., Huang, Z., Li, W., Li, Z., Song, X., Liu, W., et al. (2022). Polarization lidar measurements of dust optical properties at the junction of the Taklimakan Desert–Tibetan plateau. *Remote Sensing*, *14*(3), 558. https://doi.org/10.3390/rs14030558

Dumont, M., Tuzet, F., Gascoin, S., Picard, G., Kutuzov, S., Lafaysse, M., et al. (2020). Accelerated snow melt in the Russian caucasus mountains after the Saharan dust outbreak in March 2018. *Journal of Geophysical Research: Earth Surface*, *125*(9), e2020JF005641. https://doi.org/10.1029/2020JF005641

Emmel, C., Knippertz, P., & Schulz, O. (2010). Climatology of convective density currents in the southern foothills of the Atlas Mountains. *Journal of Geophysical Research*, *115*(D11), D11115. https://doi.org/10.1029/2009JD012863

Fleming, Z. L., Monks, P. S., & Manning, A. J. (2012). Review: Untangling the influence of air-mass history in interpreting observed atmospheric composition. *Atmospheric Research*, *104–105*, 1–39. https://doi.org/10.1016/j.atmosres.2011.09.009

Gamo, M. (1996). Thickness of the dry convection and large-scale subsidence above deserts. *Boundary-Layer Meteorology*, *79*(3), 265–278. https://doi.org/10.1007/BF00119441

Ganor, E., & Mamane, Y. (1982). Transport of Saharan dust across the eastern Mediterranean. *Atmospheric Environment (1967)*, *16*(3), 581–587. https://doi.org/10.1016/0004-6981(82)90167-6

Ha, K.-J., Moon, S., Timmermann, A., & Kim, D. (2020). Future changes of summer monsoon characteristics and evaporative demand over Asia in CMIP6 simulations. *Geophysical Research Letters*, *47*(8), e2020GL087492. https://doi.org/10.1029/2020GL087492

Han, Y., Fang, X., Zhao, T., Bai, H., Kang, S., & Song, L. (2009). Suppression of precipitation by dust particles originated in the Tibetan Plateau. *Atmospheric Environment*, *43*(3), 568–574. https://doi.org/10.1016/j.atmosenv.2008.10.018

Hoose, C., & Möhler, O. (2012). Heterogeneous ice nucleation on atmospheric aerosols: A review of results from laboratory experiments. *Atmospheric Chemistry and Physics*, *12*(20), 9817–9854. https://doi.org/10.5194/acp-12-9817-2012

Hsu, S.-C., Huh, C.-A., Lin, C.-Y., Chen, W.-N., Mahowald, N. M., Liu, S.-C., et al. (2012). Dust transport from non-East Asian sources to the North Pacific. *Geophysical Research Letters*, *39*(12), L12804. https://doi.org/10.1029/2012gl051962

Hu, Z., Huang, J., Zhao, C., Bi, J., Jin, Q., Qian, Y., et al. (2019). Modeling the contributions of Northern Hemisphere dust sources to dust outflow from East Asia. *Atmospheric Environment*, *202*, 234–243. https://doi.org/10.1016/j.atmosenv.2019.01.022

Hu, Z., Huang, J., Zhao, C., Jin, Q., Ma, Y., & Yang, B. (2020). Modeling dust sources, transport, and radiative effects at different altitudes over the Tibetan Plateau. *Atmospheric Chemistry and Physics*, *20*(3), 1507–1529. https://doi.org/10.5194/acp-20-1507-2020

Hu, Z., Huang, J., Zhao, C., Ma, Y., Jin, Q., Qian, Y., et al. (2019). Trans-pacific transport and evolution of aerosols: Spatiotemporal characteristics and source contributions. *Atmospheric Chemistry and Physics*, *19*(19), 12709–12730. https://doi.org/10.5194/acp-19-12709-2019

Hu, Z., Zhao, C., Huang, J., Leung, L. R., Qian, Y., Yu, H., et al. (2016). Trans-pacific transport and evolution of aerosols: Evaluation of quasi-global WRF-chem simulation with multiple observations. *Geoscientific Model Development*, *9*(5), 1725–1746. https://doi.org/10.5194/gmd-9-1725-2016

Hu, Z., Zhao, C., Leung, L. R., Du, Q., Ma, Y., Hagos, S., et al. (2022). Characterizing the impact of atmospheric rivers on aerosols in the Western U.S. *Geophysical Research Letters*, *49*(7), e2021GL096421. https://doi.org/10.1029/2021GL096421

Huang, J., Fu, Q., Su, J., Tang, Q., Minnis, P., Hu, Y., et al. (2009). Taklimakan dust aerosol radiative heating derived from CALIPSO observations using the Fu-Liou radiation model with CERES constraints. *Atmospheric Chemistry and Physics*, *9*(12), 4011–4021. https://doi.org/10.5194/acp-9-4011-2009

Huang, J., Lin, B., Minnis, P., Wang, T., Wang, X., Hu, Y., et al. (2006). Satellite-based assessment of possible dust aerosols semi-direct effect on cloud water path over East Asia. *Geophysical Research Letters*, *33*(19), L19802. https://doi.org/10.1029/2006GL026561

Huang, J., Minnis, P., Chen, B., Huang, Z., Liu, Z., Zhao, Q., et al. (2008). Long-range transport and vertical structure of Asian dust from CALIPSO and surface measurements during PACDEX. *Journal of Geophysical Research*, *113*(D23), D23212. https://doi.org/10.1029/2008JD010620

Huang, J., Minnis, P., Yi, Y., Tang, Q., Wang, X., Hu, Y., et al. (2007). Summer dust aerosols detected from CALIPSO over the Tibetan Plateau. *Geophysical Research Letters*, *34*(18), L18805. https://doi.org/10.1029/2007GL029938

Huang, J., Wang, T., Wang, W., Li, Z., & Yan, H. (2014). Climate effects of dust aerosols over East Asian arid and semiarid regions. *Journal of Geophysical Research: Atmospheres*, *119*(19), 11398–11416. https://doi.org/10.1002/2014JD021796

Huang, Z., Huang, J., Bi, J., Wang, G., Wang, W., Fu, Q., et al. (2010). Dust aerosol vertical structure measurements using three MPL lidars during 2008 China-U.S. joint dust field experiment. *Journal of Geophysical Research*, *115*(D7), D00K15. https://doi.org/10.1029/2009JD013273

Huang, Z., Huang, J., Hayasaka, T., Wang, S., Zhou, T., & Jin, H. (2015). Short-cut transport path for Asian dust directly to the Arctic: A case study. *Environmental Research Letters*, *10*(11), 114018. https://doi.org/10.1088/1748-9326/10/11/114018

Huang, Z., Nee, J.-B., Chiang, C.-W., Zhang, S., Jin, H., Wang, W., & Zhou, T. (2018). Real-time observations of dust–cloud interactions based on polarization and Raman lidar measurements. *Remote Sensing*, *10*(7), 1017. https://doi.org/10.3390/rs10071017

Huang, Z., Qi, S., Zhou, T., Dong, Q., Ma, X., Zhang, S., et al. (2020). Investigation of aerosol absorption with dual-polarization lidar observations. *Optics Express*, *28*(5), 7028–7035. https://doi.org/10.1364/oe.390475

Huang, Z., Wang, Y., Bi, J., Wang, T., Li, W., Li, Z., & Zhou, T. (2022). *An overview of aerosol lidar: progress and prospect*, *26*(5), 834–851. https://doi.org/10.11834/jrs.20221388

Huneeus, N., Schulz, M., Balkanski, Y., Griesfeller, J., Prospero, J., Kinne, S., et al. (2011). Global dust model intercomparison in AeroCom phase I. *Atmospheric Chemistry and Physics*, *11*(15), 7781–7816. https://doi.org/10.5194/acp-11-7781-2011

Kalnay, E., Kanamitsu, M., Kistler, R., Collins, W., Deaven, D., Gandin, L., et al. (1996). The NCEP/NCAR 40-year reanalysis project. *Bulletin of the American Meteorological Society*, *77*(3), 437–472. https://doi.org/10.1175/1520-0477(1996)077<0437:Tnyrp>2.0.Co;2

Kanamitsu, M. (1989). Description of the NMC global data assimilation and Forecast system. *Weather and Forecasting*, *4*(3), 335–342. https://doi.org/10.1175/1520-0434(1989)004<0335:DOTNGD>2.0.CO;2

Karydis, V. A., Kumar, P., Barahona, D., Sokolik, I. N., & Nenes, A. (2011). On the effect of dust particles on global cloud condensation nuclei and cloud droplet number. *Journal of Geophysical Research*, *116*(D23). https://doi.org/10.1029/2011JD016283

Kaufman, Y. J., Koren, I., Remer, L. A., Tanré, D., Ginoux, P., & Fan, S. (2005). Dust transport and deposition observed from the Terra-Moderate Resolution Imaging Spectroradiometer (MODIS) spacecraft over the Atlantic Ocean. *Journal of Geophysical Research*, *110*(D10), D10S12. https://doi.org/10.1029/2003JD004436

Kim, S.-W., Yoon, S.-C., Kim, J., & Kim, S.-Y. (2007). Seasonal and monthly variations of columnar aerosol optical properties over east Asia determined from multi-year MODIS, LIDAR, and AERONET Sun/sky radiometer measurements. *Atmospheric Environment*, *41*(8), 1634–1651. https://doi.org/10.1016/j.atmosenv.2006.10.044

Kistler, R., Kalnay, E., Collins, W., Saha, S., White, G., Woollen, J., et al. (2001). The NCEP–NCAR 50-year reanalysis: Monthly means CD-ROM and documentation. *Bulletin of the American Meteorological Society*, *82*(2), 247–268. https://doi.org/10.1175/1520-0477(2001)082<0247:TNNYRM>2.3.CO;2

Knippertz, P., Deutscher, C., Kandler, K., Müller, T., Schulz, O., & Schütz, L. (2007). Dust mobilization due to density currents in the Atlas region: Observations from the Saharan mineral dust experiment 2006 field campaign. *Journal of Geophysical Research*, *112*(D21), D21109. https://doi.org/10.1029/2007JD008774

Knippertz, P., & Todd, M. C. (2012). Mineral dust aerosols over the Sahara: Meteorological controls on emission and transport and implications for modeling. *Reviews of Geophysics*, *50*(1), RG1007. https://doi.org/10.1029/2011RG000362

Koch, J., & Renno, N. O. (2005). The role of convective plumes and vortices on the global aerosol budget. *Geophysical Research Letters*, *32*(18). https://doi.org/10.1029/2005GL023420

Koehler, K. A., Kreidenweis, S. M., DeMott, P. J., Petters, M. D., Prenni, A. J., & Carrico, C. M. (2009). Hygroscopicity and cloud droplet activation of mineral dust aerosol. *Geophysical Research Letters*, *36*(8), L08805. https://doi.org/10.1029/2009GL037348

Kuang, X., & Zhang, Y. (2005). Seasonal variation of the East Asian Subtropical westerly jet and its association with the heating field over East Asia. *Advances in Atmospheric Sciences*, *22*(6), 831–840. https://doi.org/10.1007/BF02918683

Kurosaki, Y., & Mikami, M. (2007). Threshold wind speed for dust emission in east Asia and its seasonal variations. *Journal of Geophysical Research*, *112*(D17), D17202. https://doi.org/10.1029/2006JD007988

Kutuzov, S., Shahgedanova, M., Mikhalenko, V., Ginot, P., Lavrentiev, I., & Kemp, S. (2013). High-resolution provenance of desert dust deposited on Mt. Elbrus, Caucasus in 2009–2012 using snow pit and firn core records. *The Cryosphere*, *7*(5), 1481–1498. https://doi.org/10.5194/tc-7-1481-2013

Lau, K.-M., & Kim, K.-M. (2006). Observational relationships between aerosol and Asian monsoon rainfall, and circulation. *Geophysical Research Letters*, *33*(21), L21810. https://doi.org/10.1029/2006GL027546

Lavaysse, C., Chaboureau, J.-P., & Flamant, C. (2011). Dust impact on the West African heat low in summertime. *Quarterly Journal of the Royal Meteorological Society*, *137*(658), 1227–1240. https://doi.org/10.1002/qj.844

Lee, H. N., Igarashi, Y., Chiba, M., Aoyama, M., Hirose, K., & Tanaka, T. (2006). Global model simulations of the transport of Asian and Sahara dust: Total deposition of dust mass in Japan. *Water, Air, and Soil Pollution*, *169*(1), 137–166. https://doi.org/10.1007/s11270-006-1895-8

Lee, K. H., Li, Z., Wong, M. S., Xin, J., Wang, Y., Hao, W.-M., & Zhao, F. (2007). Aerosol single scattering albedo estimated across China from a combination of ground and satellite measurements. *Journal of Geophysical Research*, *112*(D22), D22S15. https://doi.org/10.1029/2007JD009077

Lee, Y. C., Yang, X., & Wenig, M. (2010). Transport of dusts from East Asian and non-East Asian sources to Hong Kong during dust storm related events 1996–2007. *Atmospheric Environment*, *44*(30), 3728–3738. https://doi.org/10.1016/j.atmosenv.2010.03.034

Leung, L. R., & Qian, Y. (2009). Atmospheric rivers induced heavy precipitation and flooding in the Western U.S. simulated by the WRF regional climate model. *Geophysical Research Letters*, *36*(3). https://doi.org/10.1029/2008GL036445

Liu, D., Wang, Z., Liu, Z., Winker, D., & Trepte, C. (2008). A height resolved global view of dust aerosols from the first year CALIPSO lidar measurements. *Journal of Geophysical Research*, *113*(D16), D16214. https://doi.org/10.1029/2007JD009776

Liu, Z., Liu, D., Huang, J., Vaughan, M., Uno, I., Sugimoto, N., et al. (2008). Airborne dust distributions over the Tibetan Plateau and surrounding areas derived from the first year of CALIPSO lidar observations. *Atmospheric Chemistry and Physics*, *8*(16), 5045–5060. https://doi.org/10.5194/acp-8-5045-2008

Liu, Z., Omar, A., Vaughan, M., Hair, J., Kittaka, C., Hu, Y., et al. (2008). CALIPSO lidar observations of the optical properties of Saharan dust: A case study of long-range transport. *Journal of Geophysical Research*, *113*(D7), D07207. https://doi.org/10.1029/2007JD008878

Ma, X., Huang, Z., Qi, S., Huang, J., Zhang, S., Dong, Q., & Wang, X. (2020). Ten-year global particulate mass concentration derived from space-borne CALIPSO lidar observations. *Science of The Total Environment*, *721*, 137699. https://doi.org/10.1016/j.scitotenv.2020.137699

Mamun, A., Chen, Y., & Liang, J. (2021). Radiative and cloud microphysical effects of the Saharan dust simulated by the WRF-Chem model. *Journal of Atmospheric and Solar-Terrestrial Physics*, *219*, 105646. https://doi.org/10.1016/j.jastp.2021.105646

Mao, R., Hu, Z., Zhao, C., Gong, D.-Y., Guo, D., & Wu, G. (2019). The source contributions to the dust over the Tibetan Plateau: A modelling analysis. *Atmospheric Environment*, *214*, 116859. https://doi.org/10.1016/j.atmosenv.2019.116859

McKendry, I. G., Strawbridge, K. B., O'Neill, N. T., Macdonald, A. M., Liu, P. S. K., Leaitch, W. R., et al. (2007). Trans-pacific transport of Saharan dust to Western North America: A case study. *Journal of Geophysical Research*, *112*(D1), D01103. https://doi.org/10.1029/2006JD007129

Mills, M. M., Ridame, C., Davey, M., La Roche, J., & Geider, R. J. (2004). Iron and phosphorus co-limit nitrogen fixation in the eastern tropical North Atlantic. *Nature*, *429*(6989), 292–294. https://doi.org/10.1038/nature02550

Pabortsava, K., Lampitt, R. S., Benson, J., Crowe, C., McLachlan, R., Le Moigne, F. A. C., et al. (2017). Carbon sequestration in the deep Atlantic enhanced by Saharan dust. *Nature Geoscience*, *10*(3), 189–194. https://doi.org/10.1038/ngeo2899

Pan, B., Wang, Y., Hu, J., Lin, Y., Hsieh, J.-S., Logan, T., et al. (2018). Impacts of Saharan dust on Atlantic regional climate and implications for tropical cyclones. *Journal of Climate*, *31*(18), 7621–7644. https://doi.org/10.1175/jcli-d-16-0776.1

Perry, K. D., Cahill, T. A., Eldred, R. A., Dutcher, D. D., & Gill, T. E. (1997). Long-range transport of North African dust to the eastern United States. *Journal of Geophysical Research*, *102*(D10), 11225–11238. https://doi.org/10.1029/97JD00260

Prospero, J. M. (1999). Long-range transport of mineral dust in the global atmosphere: Impact of African dust on the environment of the southeastern United States. *Proceedings of the National Academy of Sciences*, *96*(7), 3396–3403. https://doi.org/10.1073/pnas.96.7.3396

Prospero, J. M., Collard, F.-X., Molinié, J., & Jeannot, A. (2014). Characterizing the annual cycle of African dust transport to the Caribbean Basin and South America and its impact on the environment and air quality. *Global Biogeochemical Cycles*, *28*(7), 757–773. https://doi.org/10.1002/2013GB004802

Prospero, J. M., Glaccum, R. A., & Nees, R. T. (1981). Atmospheric transport of soil dust from Africa to South America. *Nature*, *289*(5798), 570–572. https://doi.org/10.1038/289570a0

Pu, B., & Jin, Q. (2021). A record-breaking trans-Atlantic African dust plume associated with atmospheric circulation extremes in June 2020. *Bulletin of the American Meteorological Society*, *102*(7), E1340–E1356. https://doi.org/10.1175/BAMS-D-21-0014.1

Reid, J. S., Westphal, D. L., Livingston, J. M., Savoie, D. L., Maring, H. B., Jonsson, H. H., et al. (2002). Dust vertical distribution in the caribbean during the Puerto Rico dust experiment. *Geophysical Research Letters*, *29*(7), 55-1–55-4. https://doi.org/10.1029/2001GL014092

Rolph, G., Stein, A., & Stunder, B. (2017). Real-time environmental applications and display sYstem: READY. *Environmental Modelling & Software*, *95*, 210–228. https://doi.org/10.1016/j.envsoft.2017.06.025

Ryder, C. L., Highwood, E. J., Walser, A., Seibert, P., Philipp, A., & Weinzierl, B. (2019). Coarse and giant particles are ubiquitous in Saharan dust export regions and are radiatively significant over the Sahara. *Atmospheric Chemistry and Physics*, *19*(24), 15353–15376. https://doi.org/10.5194/acp-19-15353-2019

Sarangi, C., Qian, Y., Rittger, K., Ruby Leung, L., Chand, D., Bormann, K. J., & Painter, T. H. (2020). Dust dominates high-altitude snow darkening and melt over high-mountain Asia. *Nature Climate Change*, *10*(11), 1045–1051. https://doi.org/10.1038/s41558-020-00909-3

Sassen, K., DeMott, P. J., Prospero, J. M., & Poellot, M. R. (2003). Saharan dust storms and indirect aerosol effects on clouds: CRYSTAL-FACE results. *Geophysical Research Letters*, *30*(12). https://doi.org/10.1029/2003GL017371

Schlesinger, P., Mamane, Y., & Grishkan, I. (2006). Transport of microorganisms to Israel during Saharan dust events. *Aerobiologia*, *22*(4), 259–273. https://doi.org/10.1007/s10453-006-9038-7

Schneider, T., Bischoff, T., & Haug, G. H. (2014). Migrations and dynamics of the intertropical convergence zone. *Nature*, *513*(7516), 45–53. https://doi.org/10.1038/nature13636

Stein, A. F., Draxler, R. R., Rolph, G. D., Stunder, B. J. B., Cohen, M. D., & Ngan, F. (2015). NOAA's HYSPLIT atmospheric transport and dispersion modeling system. *Bulletin of the American Meteorological Society*, *96*(12), 2059–2077. https://doi.org/10.1175/bams-d-14-00110.1

Stein, A. F., Rolph, G. D., Draxler, R. R., Stunder, B., & Ruminski, M. (2009). Verification of the NOAA smoke forecasting system: Model sensitivity to the injection height. *Weather and Forecasting*, *24*(2), 379–394. https://doi.org/10.1175/2008waf2222166.1

Stohl, A. (1998). Computation, accuracy and applications of trajectories—A review and bibliography. *Atmospheric Environment*, *32*(6), 947–966. https://doi.org/10.1016/S1352-2310(97)00457-3

Strong, J. D. O., Vecchi, G. A., & Ginoux, P. (2018). The climatological effect of Saharan dust on global tropical cyclones in a fully coupled GCM. *Journal of Geophysical Research: Atmospheres*, *123*(10), 5538–5559. https://doi.org/10.1029/2017JD027808

Sugimoto, N., & Huang, Z. (2014). Lidar methods for observing mineral dust. *Journal of Meteorological Research*, *28*(2), 173–184. https://doi.org/10.1007/s13351-014-3068-9

Sun, H., Pan, Z., & Liu, X. (2012). Numerical simulation of spatial-temporal distribution of dust aerosol and its direct radiative effects on East Asian climate. *Journal of Geophysical Research*, *117*(D13). https://doi.org/10.1029/2011JD017219

Tanaka, T. Y., & Chiba, M. (2006). A numerical study of the contributions of dust source regions to the global dust budget. *Global and Planetary Change*, *52*(1), 88–104. https://doi.org/10.1016/j.gloplacha.2006.02.002

Tanaka, T. Y., Kurosaki, Y., Chiba, M., Matsumura, T., Nagai, T., Yamazaki, A., et al. (2005). Possible transcontinental dust transport from North Africa and the Middle East to East Asia. *Atmospheric Environment*, *39*(21), 3901–3909. https://doi.org/10.1016/j.atmosenv.2005.03.034

Thorncroft, C. D., & Blackburn, M. (1999). Maintenance of the African easterly jet. *Quarterly Journal of the Royal Meteorological Society*, *125*(555), 763–786. https://doi.org/10.1002/qj.49712555502

Tian, Y., Wang, Z., Pan, X., Li, J., Yang, T., Wang, D., et al. (2020). Influence of the morphological change in natural Asian dust during transport: A modeling study for a typical dust event over Northern China. *Science of The Total Environment*, *739*, 139791. https://doi.org/10.1016/j.scitotenv.2020.139791

Twohy, C. H., Anderson, B. E., Ferrare, R. A., Sauter, K. E., L'Ecuyer, T. S., van den Heever, S. C., et al. (2017). Saharan dust, convective lofting, aerosol enhancement zones, and potential impacts on ice nucleation in the tropical upper troposphere. *Journal of Geophysical Research: Atmospheres*, *122*(16), 8833–8851. https://doi.org/10.1002/2017JD026933

Uno, I., Eguchi, K., Yumimoto, K., Liu, Z., Hara, Y., Sugimoto, N., et al. (2011). Large Asian dust layers continuously reached North America in April 2010. *Atmospheric Chemistry and Physics*, *11*(14), 7333–7341. https://doi.org/10.5194/acp-11-7333-2011

Uno, I., Eguchi, K., Yumimoto, K., Takemura, T., Shimizu, A., Uematsu, M., et al. (2009). Asian dust transported one full circuit around the globe. *Nature Geoscience*, *2*(8), 557–560. https://doi.org/10.1038/ngeo583

Winker, D. M., Hunt, W. H., & McGill, M. J. (2007). Initial performance assessment of CALIOP. *Geophysical Research Letters*, *34*(19), L19803. https://doi.org/10.1029/2007GL030135

Winker, D. M., Pelon, J., Coakley, J. A., Ackerman, S. A., Charlson, R. J., Colarco, P. R., et al. (2010). The CALIPSO mission: A global 3D view of aerosols and clouds. *Bulletin of the American Meteorological Society*, *91*(9), 1211–1230. https://doi.org/10.1175/2010BAMS3009.1

Winker, D. M., Vaughan, M. A., Omar, A., Hu, Y., Powell, K. A., Liu, Z., et al. (2009). Overview of the CALIPSO mission and CALIOP data processing algorithms. *Journal of Atmospheric and Oceanic Technology*, *26*(11), 2310–2323. https://doi.org/10.1175/2009jtecha1281.1

Xin, J., Wang, Y., Li, Z., Wang, P., Hao, W. M., Nordgren, B. L., et al. (2007). Aerosol optical depth (AOD) and Ångström exponent of aerosols observed by the Chinese Sun Hazemeter network from August 2004 to September 2005. *Journal of Geophysical Research*, *112*(D5), D05203. https://doi.org/10.1029/2006JD007075

Yin, Y., & Chen, L. (2007). The effects of heating by transported dust layers on cloud and precipitation: A numerical study. *Atmospheric Chemistry and Physics*, *7*(13), 3497–3505. https://doi.org/10.5194/acp-7-3497-2007

Yin, Z., Wan, Y., Zhang, Y., & Wang, H. (2021). Why super sandstorm 2021 in North China. *National Science Review*, *9*(3). https://doi.org/10.1093/nsr/nwab165

Yu, H., Chin, M., Bian, H., Yuan, T., Prospero, J. M., Omar, A. H., et al. (2015). Quantification of trans-Atlantic dust transport from seven-year (2007–2013) record of CALIPSO lidar measurements. *Remote Sensing of Environment*, *159*, 232–249. https://doi.org/10.1016/j.rse.2014.12.010

Yu, H., Chin, M., Yuan, T., Bian, H., Remer, L. A., Prospero, J. M., et al. (2015). The fertilizing role of African dust in the Amazon rainforest: A first multiyear assessment based on data from cloud-aerosol lidar and infrared pathfinder satellite observations. *Geophysical Research Letters*, *42*(6), 1984–1991. https://doi.org/10.1002/2015GL063040

Yu, H., Remer, L. A., Chin, M., Bian, H., Kleidman, R. G., & Diehl, T. (2008). A satellite-based assessment of transpacific transport of pollution aerosol. *Journal of Geophysical Research*, *113*(D14), D14S12. https://doi.org/10.1029/2007JD009349

Yu, H., Tan, Q., Chin, M., Remer, L. A., Kahn, R. A., Bian, H., et al. (2019). Estimates of African dust deposition along the trans-Atlantic transit using the decadelong record of aerosol measurements from CALIOP, MODIS, MISR, and IASI. *Journal of Geophysical Research: Atmospheres*, *124*(14), 7975–7996. https://doi.org/10.1029/2019JD030574

Yu, Y., Kalashnikova, O. V., Garay, M. J., Lee, H., Notaro, M., Campbell, J. R., et al. (2020). Disproving the Bodélé depression as the primary source of dust fertilizing the Amazon rainforest. *Geophysical Research Letters*, *47*(13), e2020GL088020. https://doi.org/10.1029/2020GL088020

Yuan, T., Huang, J., Cao, J., Zhang, G., & Ma, X. (2021). Indian dust-rain storm: Possible influences of dust ice nuclei on deep convective clouds. *Science of The Total Environment*, *779*, 146439. https://doi.org/10.1016/j.scitotenv.2021.146439

Yumimoto, K., Eguchi, K., Uno, I., Takemura, T., Liu, Z., Shimizu, A., et al. (2010). Summertime trans-Pacific transport of Asian dust. *Geophysical Research Letters*, *37*(18). https://doi.org/10.1029/2010GL043995

Zhang, S., Huang, Z., Li, M., Shen, X., Wang, Y., Dong, Q., et al. (2022). Vertical structure of dust aerosols observed by a ground-based Raman lidar with polarization capabilities in the center of the Taklimakan Desert. *Remote Sensing*, *14*(10), 2461. https://doi.org/10.3390/rs14102461

Zhang, Z., Zhou, W., Wenig, M., & Yang, L. (2017). Impact of long-range desert dust transport on hydrometeor formation over coastal East Asia. *Advances in Atmospheric Sciences*, *34*(1), 101–115. https://doi.org/10.1007/s00376-016-6157-0

Zhao, C., Chen, S., Leung, L. R., Qian, Y., Kok, J. F., Zaveri, R. A., & Huang, J. (2013). Uncertainty in modeling dust mass balance and radiative forcing from size parameterization. *Atmospheric Chemistry and Physics*, *13*(21), 10733–10753. https://doi.org/10.5194/acp-13-10733-2013

Zhao, C., & Zhang, M. S. (2021). mszhang96/wrfchem_ustc: WRF-Chem_MEGANv3.0 (v1.0) [Software]. Zenodo. https://doi.org/10.5281/zenodo.4663508

References From the Supporting Information

Binkowski, F. S., & Shankar, U. (1995). The regional particulate Matter Model: 1. Model description and preliminary results. *Journal of Geophysical Research*, *100*(D12), 26191–26209. https://doi.org/10.1029/95JD02093

Chapman, E. G., Gustafson, W. I., Jr., Easter, R. C., Barnard, J. C., Ghan, S. J., Pekour, M. S., & Fast, J. D. (2009). Coupling aerosol-cloud-radiative processes in the WRF-Chem model: Investigating the radiative impact of elevated point sources. *Atmospheric Chemistry and Physics*, *9*(3), 945–964. https://doi.org/10.5194/acp-9-945-2009

Easter, R. C., Ghan, S. J., Zhang, Y., Saylor, R. D., Chapman, E. G., Laulainen, N. S., et al. (2004). MIRAGE: Model description and evaluation of aerosols and trace gases. *Journal of Geophysical Research*, *109*(D20), D20210. https://doi.org/10.1029/2004JD004571

Fast, J. D., Gustafson, W. I., Jr., Easter, R. C., Zaveri, R. A., Barnard, J. C., Chapman, E. G., et al. (2006). Evolution of ozone, particulates, and aerosol direct radiative forcing in the vicinity of Houston using a fully coupled meteorology-chemistry-aerosol model. *Journal of Geophysical Research*, *111*(D21), D21305. https://doi.org/10.1029/2005JD006721

Ginoux, P., Chin, M., Tegen, I., Prospero, J. M., Holben, B., Dubovik, O., & Lin, S.-J. (2001). Sources and distributions of dust aerosols simulated with the GOCART model. *Journal of Geophysical Research*, *106*(D17), 20255–20273. https://doi.org/10.1029/2000JD000053

Iacono, M. J., Mlawer, E. J., Clough, S. A., & Morcrette, J.-J. (2000). Impact of an improved longwave radiation model, RRTM, on the energy budget and thermodynamic properties of the NCAR community climate model, CCM3. *Journal of Geophysical Research*, *105*(D11), 14873–14890. https://doi.org/10.1029/2000JD900091

Mlawer, E. J., Taubman, S. J., Brown, P. D., Iacono, M. J., & Clough, S. A. (1997). Radiative transfer for inhomogeneous atmospheres: RRTM, a validated correlated-k model for the longwave. *Journal of Geophysical Research*, *102*(D14), 16663–16682. https://doi.org/10.1029/97JD00237

Stauffer, D. R., & Seaman, N. L. (1990). Use of four-dimensional data assimilation in a limited-area mesoscale model. Part I: Experiments with synoptic-scale data. *Monthly Weather Review*, *118*(6), 1250–1277. https://doi.org/10.1175/1520-0493(1990)118<1250:UOFDDA>2.0.CO;2

Zaveri, R. A., Easter, R. C., Fast, J. D., & Peters, L. K. (2008). Model for simulating aerosol interactions and chemistry (MOSAIC). *Journal of Geophysical Research*, *113*(D13), D13204. https://doi.org/10.1029/2007JD008782

Zaveri, R. A., & Peters, L. K. (1999). A new lumped structure photochemical mechanism for large-scale applications. *Journal of Geophysical Research*, *104*(D23), 30387–30415. https://doi.org/10.1029/1999JD900876

Zhao, C., Liu, X., Leung, L. R., Johnson, B., McFarlane, S. A., Gustafson, W. I., Jr., et al. (2010). The spatial distribution of mineral dust and its shortwave radiative forcing over North Africa: Modeling sensitivities to dust emissions and aerosol size treatments. *Atmospheric Chemistry and Physics*, *10*(18), 8821–8838. https://doi.org/10.5194/acp-10-8821-2010

Zhao, C., Liu, X., Ruby Leung, L., & Hagos, S. (2011). Radiative impact of mineral dust on monsoon precipitation variability over West Africa. *Atmospheric Chemistry and Physics*, *11*(5), 1879–1893. https://doi.org/10.5194/acp-11-1879-2011

Zhao, C., Ruby Leung, L., Easter, R., Hand, J., & Avise, J. (2013). Characterization of speciated aerosol direct radiative forcing over California. *Journal of Geophysical Research: Atmospheres*, *118*(5), 2372–2388. https://doi.org/10.1029/2012JD018364